WIDEBAND ROTARY TRANSFORMER FOR VHF USE

by

Charles W. Allen

Dissertation submitted to the Graduate Faculty of the
Virginia Polytechnic Institute and State University
in partial fulfillment of the requirements for the degree of

DOCTOR OF PHILOSOPHY

in

Electrical Engineering

APPROVED:

H. L. Krauss, Chairman

C. A. Holt

E. A. Manus

L. H. Slack

W. A. Blackwell

August, 1975

Blacksburg, Virginia

ACKNOWLEDGMENT

The author wishes to thank his committee, and in particular Dr. H. L. Krauss, for the guidance he received during the course of this research. Also, thanks should be extended to Mr. Joe Fowler and Mr. Meredith Hamilton at NASA Houston who made the construction of a prototype device possible.

The support received through Dr. W. A. Blackwell and Virginia Polytechnic Institute and State University is also gratefully acknowledged. And last, sincere appreciation is extended to Mrs. Vickie F. Carroll for doing an excellent job in typing this manuscript.

TABLE OF CONTENTS

LIST OF FIGURES

LIST OF FIGURES (continued)

LIST OF FIGURES (continued)

LIST OF FIGURES (continued)

LIST OF SYMBOLS

A_e - Effective core cross-sectional area

A_ℓ - Inductance index

D - Center to center wire separation

d - Transmission line wire diameter

f - Frequency ($\omega/2\pi$)

f_l - Lower cutoff frequency

I - Current

j - $\sqrt{-1}$

L_e - Average core magnetic path length

L_m - Magnetizing inductance

ℓ - Transmission line length

ℓ_a, ℓ_b - Lengths of transmission lines formed during rotation of a turn

ℓ_T - Total line length of rotary transmission line

N - Number of turns on rotary transformer winding

N_p - Number of primary turns of static wideband transformer

P_{av} - Available power

P_o - Output power to load

P_{in} - Input power to rotary transformer terminals

P_{loss} - Transformer loss

R_L - Load resistance

LIST OF SYMBOLS (continued)

R_p - Core loss resistance

R_S - Source resistance

V - Voltage

V_S - Source voltage

V_p - Balanced mode phase velocity

V_u - Unbalanced mode phase velocity

X_m - Magnetizing reactance

Z_i - Input impedance of rotary transformer

Z_{in} - Input impedance corrected for parasitics

Z_a - Parasitic shunt impedance

Z_L - Load impedance

Z_o - Balanced mode characteristic impedance

Z_u - Unbalanced mode characteristic impedance

α - Balanced mode attenuation constant

α_u - Unbalanced mode attenuation constant

β - Balanced mode phase constant

β_u - Unbalanced mode phase constant

λ - Wavelength

γ_o - Balanced mode propagation constant

γ_u - Unbalanced mode propagation constant

μ_o - Relative permeability of core

ε_r - Relative dielectric permittivity

ω - Frequency in radians/sec

LIST OF SYMBOLS (continued)

θ - Rotation angle

$\tan \delta$ - Core loss tangent

[ABCD] - Transmission matrix

$|\ |$ - Magnitude

LIST OF TABLES

I. INTRODUCTION

Rotating joints or wrap-around cables which are often necessary for the transfer of RF energy across rotating structures, are inherently subject to noise, wear, and fatigue. Conventional rotary joints consist of some form of rotating coaxial transmission line or slip-ring configuration. Contact wear or material fatigue caused by device usage introduces noise and discontinuities into an RF system. In the case of wrap-around cables, continuous rotation is not possible and cable flexure eventually leads to material failure. The aforementioned problems can be reduced if the mechanical connection between the stator and rotor parts of the joint is eliminated.

A wide-band transformer has been investigated by Ruthroff [1] and more recently by Pitzalis, Horn, and Baranello [2, 3] this transformer consists of a two-wire transmission line wound upon a ferrite core. The device works well at low frequencies due to the high permeability available with ferrite materials. At higher frequencies the permeability of the core decreases, and conventional transformer action becomes less effective. Nevertheless, the two windings are coupled as a transmission line, and the device still behaves as a transformer. Chapter I of this dissertation introduces the design procedure for the static transmission line transformer.

An extension of the static transformer is then considered for application as a rotary joint. This device has transformer coupling between a rotating secondary (rotor) winding and a stationary primary (stator) winding. The two windings are arranged so that they form a two-wire transmission line circuit for high frequency coupling. A ferrite core provides low frequency coupling.

It is the purpose of this dissertation to detail the theory and construction of this type of rotating joint. Balanced and unbalanced transmission line analysis will be applied for several possible connections. For either case a theoretical consideration is facilitated by computer-aided numerical analysis. The results are then compared to the performance of an experimental device.

II. STATIC BROADBAND TRANSFORMER DESIGN TECHNIQUES

Wideband transformers that utilize two-wire or coaxial transmission lines wound on a toroidal core have been known for many years, but it is only in the last decade that they have seen extensive application in radio transmitters and instrumentation. These transformers can have bandwidths on the order of 1000:1, and are useful in the RF range. However, the design criteria and details of construction are generally omitted in current literature, so that the designer who encounters such a transformer for the first time finds it difficult to get started. The following discussion will be a helpful introduction to the ideas applied to the rotary transformer.

Ruthroff [1] and others [2, 3] have investigated a transformer consisting of a bifilar winding wound upon a ferrite toroidal core as shown in Figure 2.1.a. For such a device, low-frequency response is dependent upon the magnetizing reactance of the primary winding. At higher frequencies, the permeability of the ferrite core decreases and conventional transformer action becomes less effective. However, the two windings are coupled as a transmission line and the device still behaves like a transformer until the line length is about 0.5 wavelength [1], with response down 3 dB at 0.3 wavelength.

Figure 2.1.a shows the winding configuration for such a transformer connected to give a 4:1 impedance transformation. The equivalent

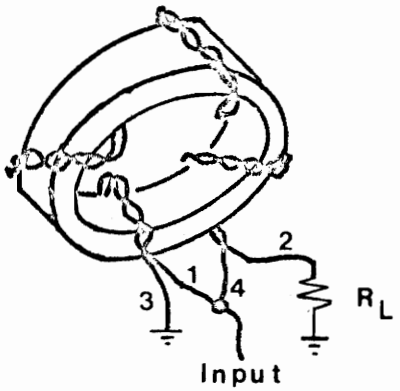

Figure 2.1.a Sketch of 4:1 transformer

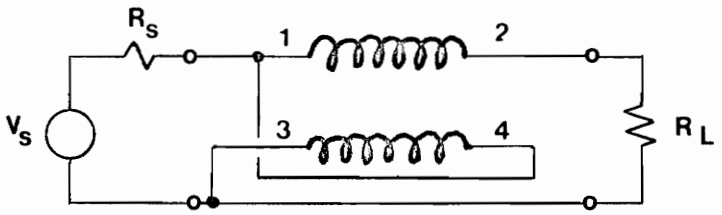

Figure 2.1.b High frequency model

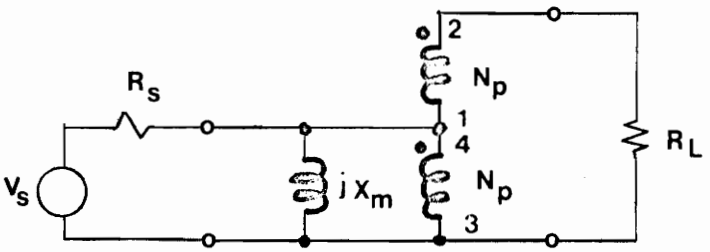

Figure 2.1.c Low frequency model

Figure 2.1 4:1 Wideband Transformer

high-frequency and low-frequency models are shown in Figure 2.1.b and 2.1.c, respectively. Other winding configurations have been discussed in the literature [2, 7, 12], but the 4:1 ratio is the one most frequently used. Also, by the addition of a few extra turns on winding 1-2, the impedance ratio can be increased up to 6:1 without serious loss of bandwidth.

2.1 Frequency Response

The available power to the transformer in Figure 2.1 is

$$P_{av} = |V_s|^2/4R_s \ , \tag{2.1}$$

in which P_{av} = available source power

V_s = source voltage

R_s = source resistance.

For the high-frequency circuit of Figure 2.1.b the insertion power loss (neglecting transmission-line loss) has been determined [1] to be

$$\frac{P_{av}}{P_o} = \frac{[2\ R_s\ (1 + \cos \beta\ell) + R_L \cos \beta\ell]^2 + \left[\frac{R_s\ R_L + Z_o^2}{Z_o}\right]^2 \sin^2 \beta\ell}{4R_L R_S\ (1 + \cos \beta\ell)^2} \ , \tag{2.2}$$

in which P_o = output power

β = transmission-line phase constant

ℓ = transmission line length

R_L = load resistance

Z_o = line characteristic impedance.

For the low-frequency circuit of Figure 2.1.c., a straightforward analysis (neglecting core loss) yields

$$P_{av}/P_o = (R_s^2 + 4\,X_m^2) \,/\, 4\,X_m^2 \,, \tag{2.3}$$

in which X_m is the primary magnetizing reactance. Maximum power transfer for these networks is obtained if

$$R_L = 4\,R_s \tag{2.4}$$

and

$$Z_o = 2\,R_s \,. \tag{2.5}$$

The core magnetizing inductance [6] is given by

$$L_m = 0.4\,\pi\,N_p^2\,\mu_o\,\frac{A_e(cm^2)}{L_e(cm)}\;X\;10^{-8}\ \text{henrys} \tag{2.6}$$

in which N_p = number of primary turns

A_e = effective cross-sectional area of the core

L_e = average magnetic path length in the core

μ_o = relative permeability of the core

L_m = magnetizing inductance (X_m/ω)

ω = frequency (radians/sec)

A composite parameter A_ℓ, defined by

$$A_\ell = 4\,\pi\,\mu_o\,(A_e/L_e) \tag{2.7}$$

and called the inductance index,

is listed by some core manufacturers [8] to simplify (2.6) such that

$$L_m = N_p^2 A_\ell \cdot 10^{-9} \text{ henrys} \tag{2.8}$$

The lower cutoff frequency, f_l, can be determined by setting (2.3) equal to 2.0 (3 dB point), giving

$$f_l = \frac{R_s \cdot 10^9}{4 \pi N_p^2 A_\ell} \text{ Hz} . \tag{2.9}$$

This relationship determines the number of turns needed for a specified low-frequency response. The upper 3 dB cutoff frequency for an optimally-matched transformer can similarly be obtained from (2.2) and occurs when the line length, ℓ, is 0.3 wavelength.

2.2 Transmission Line Considerations

The choice of the transmission-line characteristic impedance must satisfy the constraints given by (2.4) and (2.5). Several useful types of transmission lines have been reported, including twisted-pair, coaxial, and stripline [4]. Twisted-pair lines are advisable where minimal winding space is available. Use of a tight twist (conveniently obtained by means of a twist drill or lathe) is advisable to obtain uniform characteristic impedance along the line. When a loosely-twisted line is wound on a core, the wires tend to have uneven spacing, thus introducing impedance variations that degrade high-frequency performance.

Figure 2.2 depicts the effect of twist count (twists per cm) on the characteristic impedance for several twisted-pair lines. The phase

velocity on these lines is also indicated. Note that the tighter twists tend to reduce the value of Z_o. Further details concerning the construction of these and other lines having lower characteristic impedance have been discussed by Pitzalis [2], Hejhall [9], and Mueller [11]. Pitzalis and Couse [4] have shown that minor deviations of Z_o from the value given by (2.5) can be tolerated.

2.3 Obtaining the Desired Bandwidth

As noted previously, the desired insertion-loss bandwidth depends upon core specifications, number of winding turns, and transmission line length. Pitzalis [2] recommended that the line length be less than 0.125 wavelength at the highest operating frequency in order to minimize the effect of mismatch on the insertion loss. The maximum useful length of a line can be estimated from phase velocity data. The desire to have a short transmission line, along with other mechanical considerations such as available winding area, generally restricts the number of turns on the core.

The previous considerations dictate that the factor A_ℓ in (2.9) be large in order to obtain a desired lower cutoff frequency with minimal turns. The value of A_ℓ is for the most part dependent upon core permeability; thus high-mu cores are useful. Care should be exercised in the choice of a core, however, since the permeability of the higher-mu cores (μ_o > 1000 or so) tends to be temperature dependent [8] and they exhibit higher loss at high frequencies.

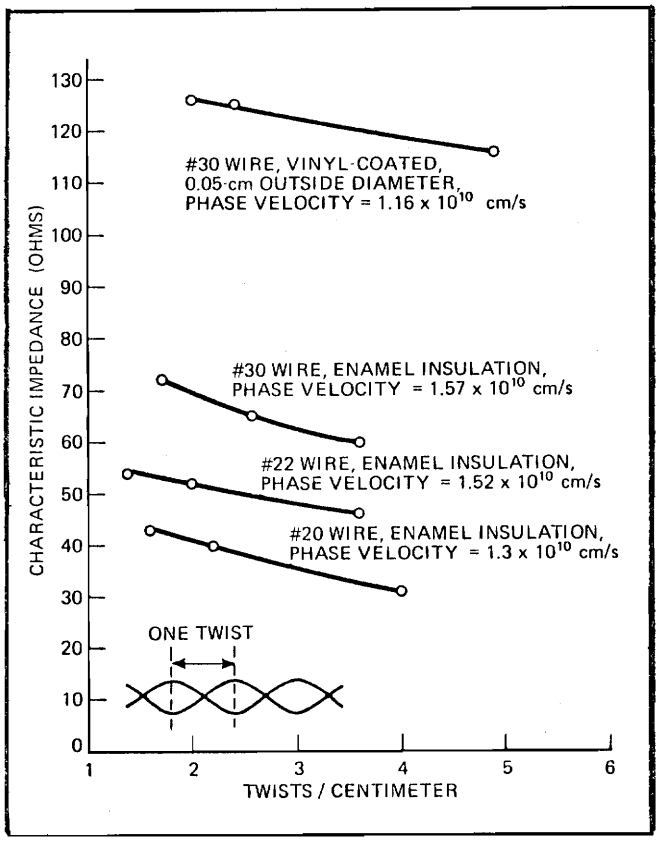

Figure 2.2 Measured data depicting characteristic impedance for twisted pair transmission line

III. THE ROTARY TRANSFORMER

The ideas pertaining to the static wideband transformer construction can be extended to a rotary joint. This device is made possible if a transmission line is made in such a fashion that one half of it is allowed to rotate with respect to its other half.

3.1 Rotary Transformer Construction

In order to construct a multiturn configuration of the rotary transformer, the stator and rotor windings are made of separate parallel turns. That is, each turn of the stator winding consists of a circular, planar turn of wire. Inside each stator turn is a corresponding concentric rotor turn which can rotate with respect to the stator. The rotor and stator wires must be mounted in some low loss dielectric medium such as nylon or plastic. The dielectric is necessary in order to maintain a fixed mechanical spacing between the windings. Finally, ferrite is then used to enclose the stator and rotor in order to form tight magnetic coupling at lower frequencies. For an illustration and photograph of the multiturn winding construction, see Figures 3.1 and 3.2. Figure 3.3 depicts the electrical connection formed during rotation in an N-turn transformer.

A two-wire transmission line is formed by each turn of the rotor and stator windings. The balanced-mode characteristic impedance, dependent upon wire diameter and separation, is approximated [18] by

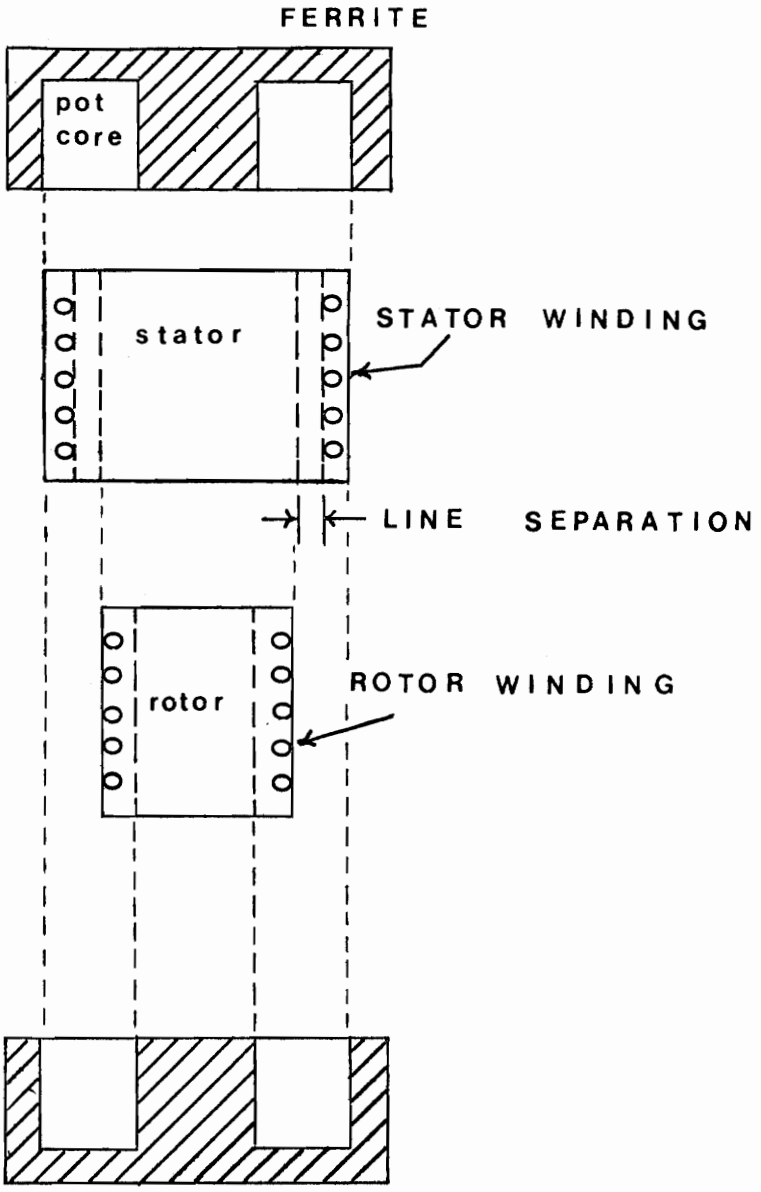

Figure 3.1 Cut-away side view of rotary transformer construction

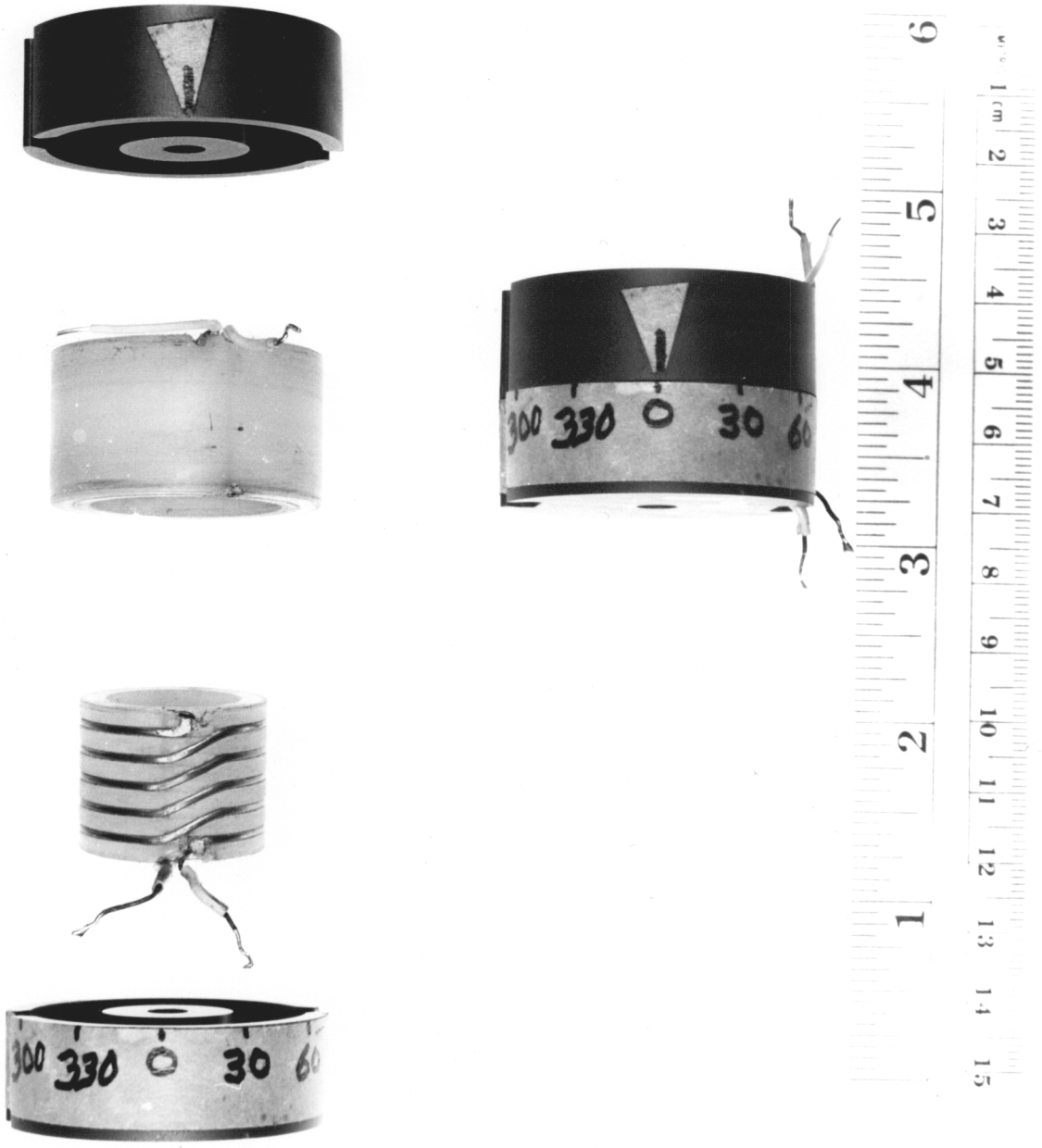

Figure 3.2 Photograph of Prototype rotating transformer

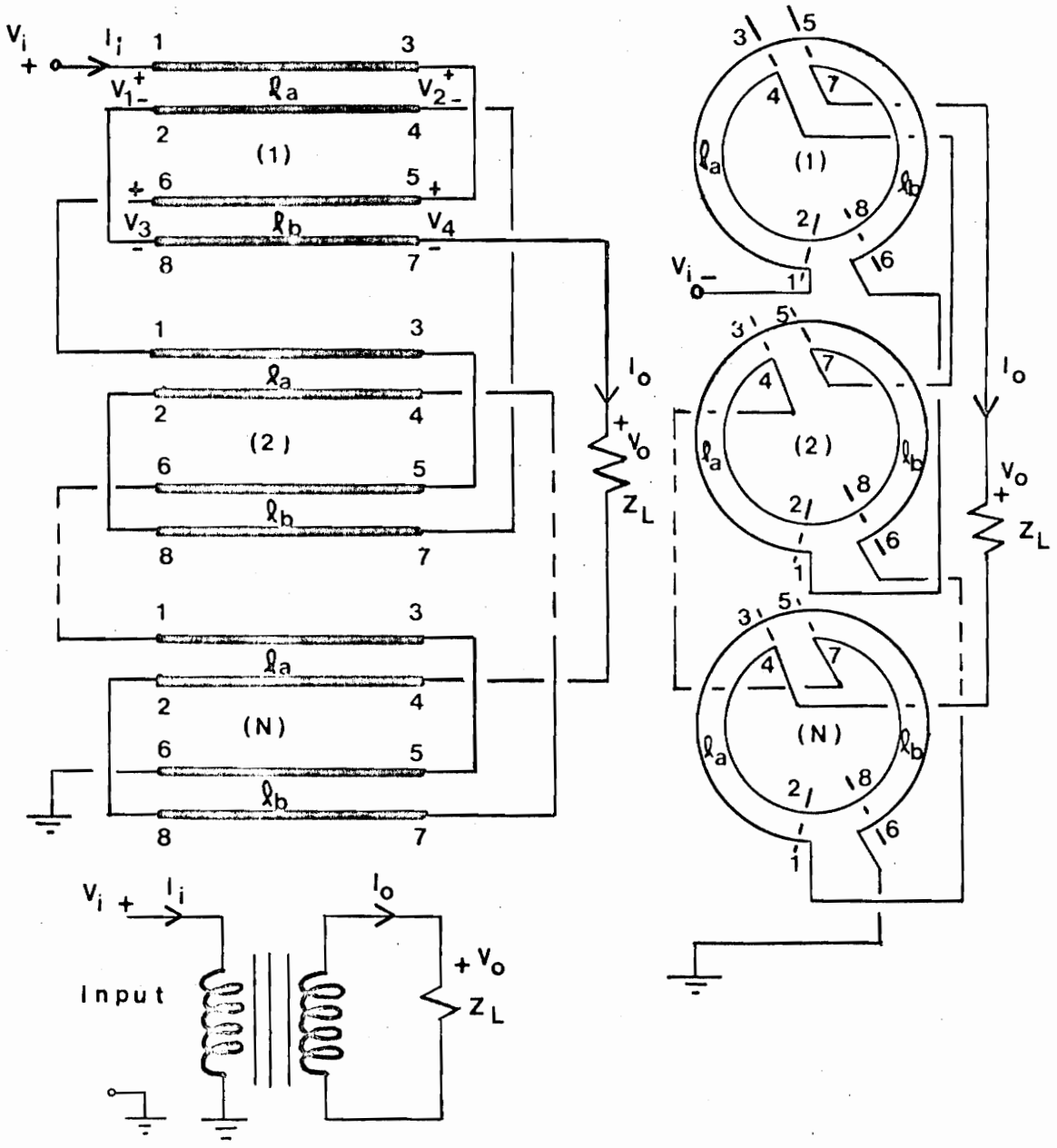

Figure 3.3 Interconnection diagram of the N-turn rotary transformer

$$Z_o = \frac{120}{\sqrt{\varepsilon_r}} \cosh^{-1} \frac{D}{d} \tag{3.1}$$

where ε_r = relative dielectric permittivity

D = center-to-center wire separation

d = wire diameter

Z_o = balanced-mode characteristic impedance

The analysis of the rotary joint is essentially the same as that for a wideband transformer except during rotation. When the transformer is rotated, two transmission-line sections of variable lengths ℓ_a and ℓ_b are formed by each turn (see Figure 3.4.a), because the terminals 4-7 of the rotor turn are not coincident with terminals 1-6 of the stator turn. The total line length, ℓ_T, for an N-turn transformer is

$$\ell_T = N(\ell_a + \ell_b) \tag{3.2}$$

The two lines formed during rotation are interconnected to those formed by other turns. All interconnections other than those of the transmission lines are assumed to be electrically short compared with the excitation wave-length.

A balanced-current transmission-line analysis simplifies the consideration of the rotary transformer. In certain cases to be discussed later, where balanced transmission line analysis fails, an unbalanced transmission line model must be used. The balanced current theory does, however, yield results which correlate with experiment in the case of an unshielded transformer having an ungrounded load (see Figure 3.3). An analysis of this configuration is provided in

Appendix A. If a ground at the load is desired, the network of Figure 3.4.b. may be used. For maximum power transfer, the optimum load impedance is

$$R_L = Z_o \tag{3.3}$$

where R_L = load resistance (pure real for a lossless line).
For this loading, the input impedance is given by

$$Z_i = Z_o \frac{N \sin \beta(\ell_a + \ell_b) + jN^2 [2 - 2 \cos \beta(\ell_a + \ell_b)]}{N \sin \beta(\ell_a + \ell_b) + j \sin \beta\ell_a \sin \beta\ell_b} \tag{3.4}$$

and the insertion loss is

$$\frac{P_{av}}{P_o} = \frac{4 N^2 \sin \beta(\ell_a + \ell_b) + \{\sin \beta\ell_a \sin \beta\ell_b + N^2[2 - 2 \cos \beta(\ell_a + \ell_b)]\}^2}{4 N^2 \{\sin^2 \beta(\ell_a + \ell_b) - [2 - 2 \cos \beta(\ell_a + \ell_b)] \sin \beta\ell_a \sin \beta\ell_b\}} \tag{3.5}$$

It is important to note that only the imaginary term in the denominator of (3.4) is a function of rotation. Also, changes in the value of this equation will be minimal if the total line length per turn in wavelengths is small. The 3 dB insertion loss point can be determined from (3.5) and occurs when $\ell_T = 0.3\lambda$, the same value predicted by (2.2) for the static transformer. The values determined from (3.5) are not affected by rotation if the rotary transformer is operated at or below the 3 dB high frequency cutoff point.

Numerically, the number of winding turns, N, will not introduce changes in the values given by (3.4) and (3.5) if the total winding length is small. Several values of N ranging from 1 to 10 were substituted into (3.4) and (3.5) and no significant changes in the results occurred with $\ell_T \leq 0.3\lambda$.

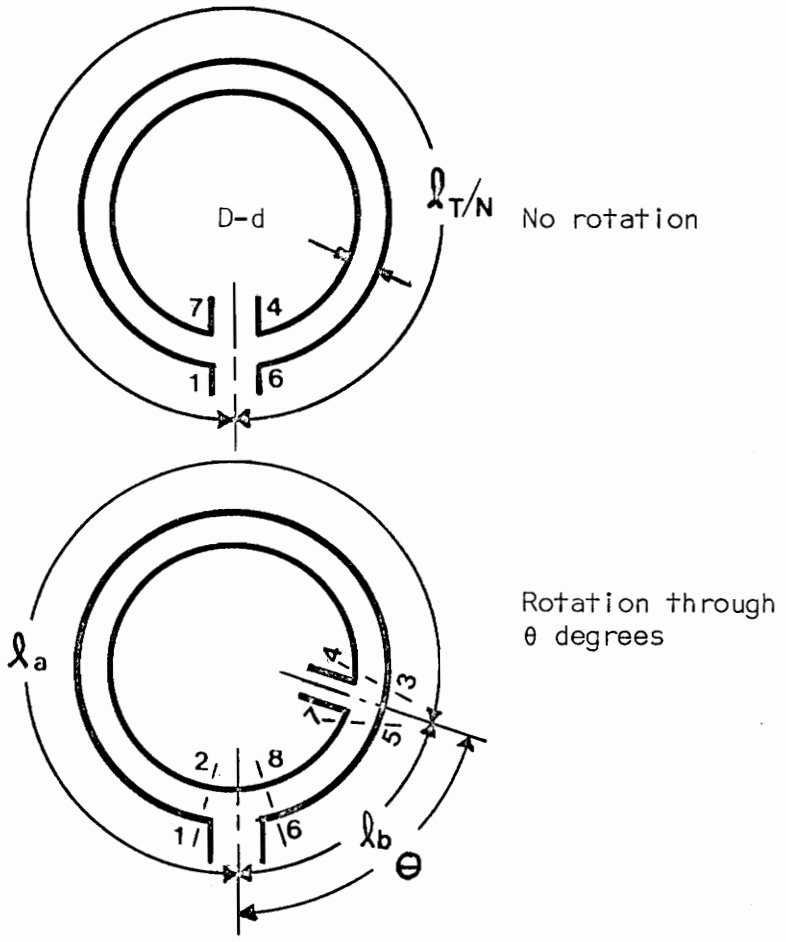

Figure 3.4.a Diagram of a rotating turn

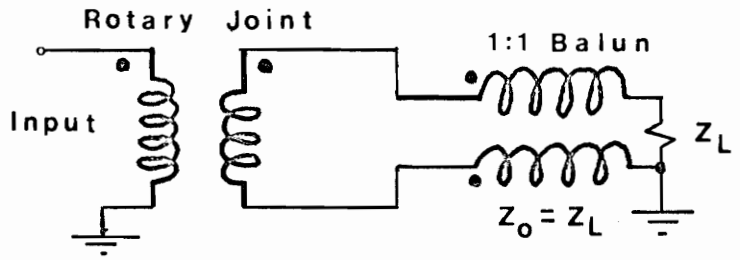

Figure 3.4.b Circuit used when the grounding of the load impedance is desired

There are parasitic shunt losses introduced into the transmission line model as in Chapter II. In particular, shunt reactance, X_m, and a shunt core loss resistance, R_p, generally must be added to the transformer circuit. These account for core losses and magnetizing reactance. In the event that shunt terms are present,

$$Z_{in} = \frac{Z_a Z_i}{Z_i + Z_a} \tag{3.6}$$

where Z_a = parasitic shunt impedance: R_p, in parallel with X_m

R_p = core loss resistance

Z_{in} = input impedance of transformer adjusted for shunt core loss and magnetizing reactance

In most cases Z_a is approximately purely reactive near the low frequency cutoff point and equation (2.2), with $N_p = N$ (the number of turns), expresses the lower cutoff frequency for the rotary transformer. At higher frequencies the core loss increases and R_p tends to dominate Z_a. Core loss-tangent data [16] will yield an estimate of R_p from the relation

$$R_p = \frac{X_m}{\tan \delta} \tag{3.7}$$

where tan δ = a tabulated loss factor (loss tangent) available as core data.

Usually, it is much more convenient to use an R-X meter to measure R_p for an actual device, since decreases in core permeability at higher frequencies cause X_m to be unpredictable. Also, R_p is somewhat dependent upon excitation levels [16].

It should be noted that R_p, if small enough, will reduce the upper cutoff frequency to some extent. It is therefore advisable to choose a transmission line characteristic impedance low enough to reduce the effects of shunt parasitics upon the input impedance so that (3.6) will reduce approximately to Z_i. Impedances on the order of 50 ohms are ideal.

3.2 Experimental Results

The behavior of a prototype rotating transformer serves to verify the previous analytical discussion. The photograph of the prototype is shown in Figure 3.2. The wideband device that was built consists of five turns with a 110 ohm transmission line. The rotor and stator were constructed of nylon and these parts were mounted in a ferrite pot core (Ferroxcube Part No. 4229P-L00-3C8). The ferrite core inductance index, A_L, was 5500. The transmission line $\beta\ell_T$ product was measured to be

$$\beta\ell_T = 0.019\ f \text{ (radians)}$$

with f given in MHz.

The measured variation of R_p versus frequency is depicted by Figure 3.5. This data was obtained with an R-X meter while the transformer was open circuited. A low frequency measurement of the open-circuit input impedance of the transformer indicated that the shunt magnetizing reactance was due to a 130 μH inductance. It was impossible to determine X_m at frequencies above 1 MHz due to shunting effects caused by interwinding capacitance. Therefore, X_m for a theoretical analysis was assumed due to a 130 μH inductance at all frequencies.

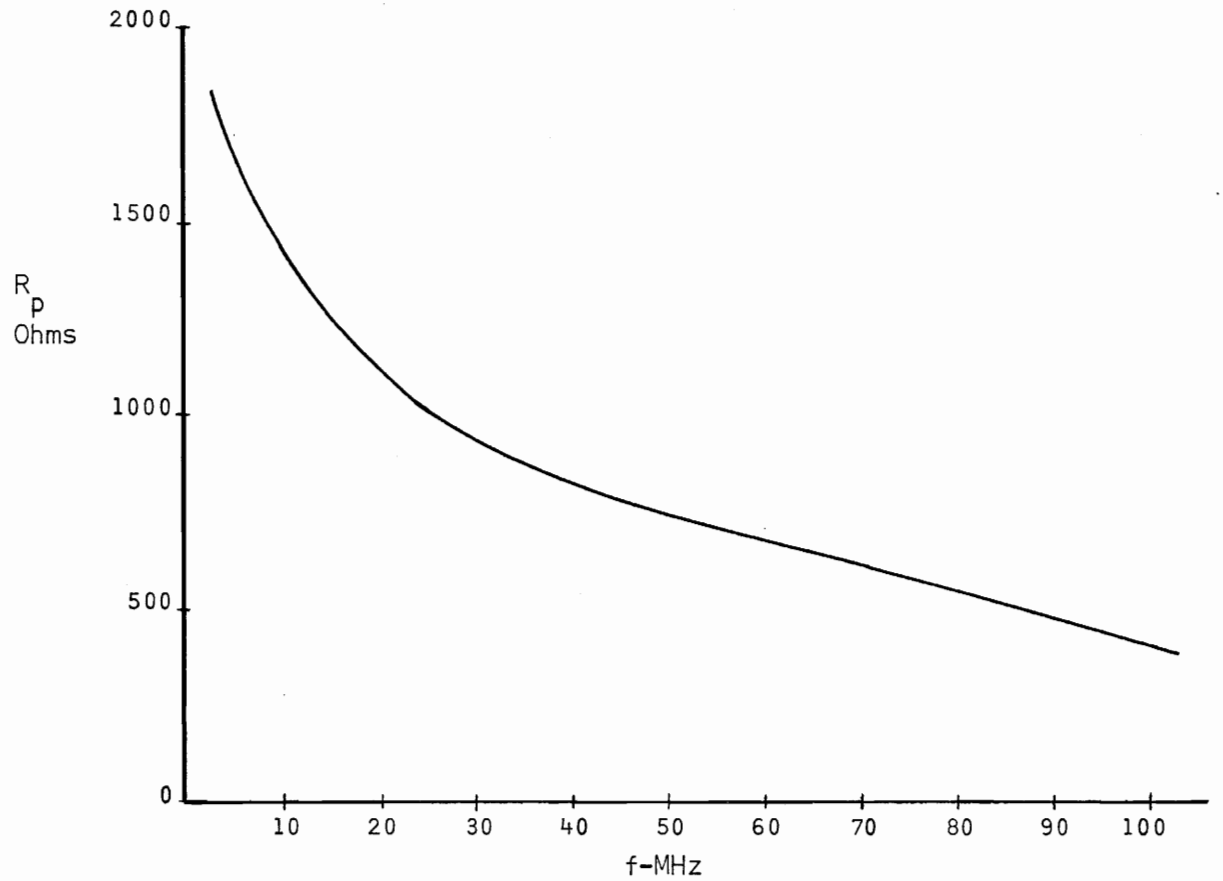

Figure 3.5 Measured shunt loss resistance, R_p, versus frequency of the rotary transformer

The reader should note that the performance of the wideband rotating joint correlates well with the theory of operation. Over the bandwidth of the device, 80-kHz to 80-MHz, there is no detectable performance change due to rotation. Consequently Figures 3.6 and 3.7 which depict the input impedance and insertion loss are accurate for 360° of rotation.

The upper cutoff frequency could be extended by winding fewer turns or decreasing the radius of the turns. Both techniques increase the lower cutoff frequency by reducing X_m. Core losses would be increased as well since they are related to the magnetizing reactance value (see (3.7)). Use of a low loss core would, however, balance this effect.

All measurements were made at low power levels. Input impedance and insertion loss measurements were made with signal power less than 10 mw.

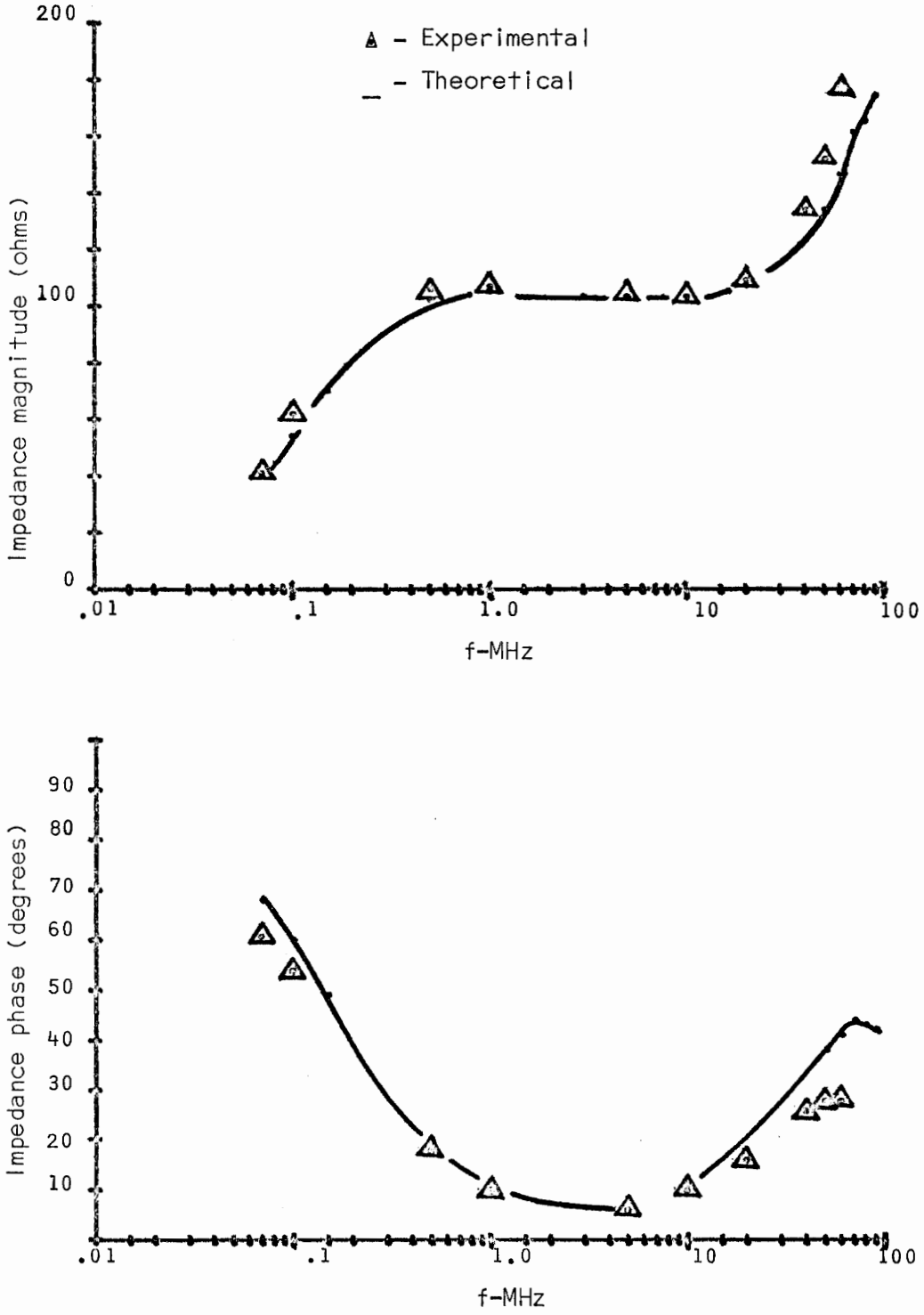

Figure 3.6 Input impedance magnitude and phase vs. frequency for the transformer terminated in $R_L = Z_o = 110$ ohms

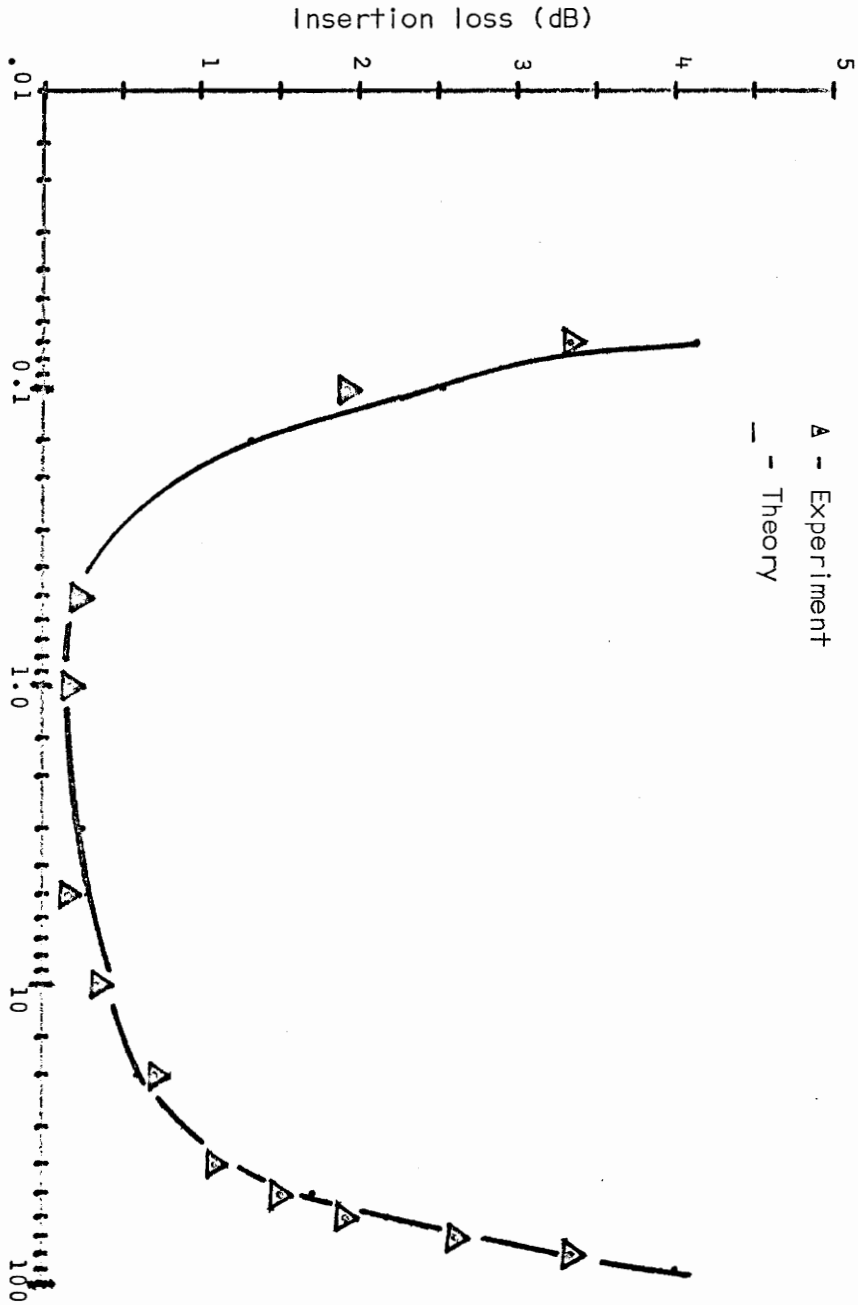

Figure 3.7 Insertion loss vs. frequency

IV. THE ANALYSIS OF TWO USEFUL CONNECTIONS

Due to the existence of an unbalanced current mode on the transmission line, a shielded rotating transformer cannot be analyzed with a balanced current approach. An adequate distributed model has been proposed by Sato [12] and others [13, 14, 15] and has been found both effective and accurate for application to the rotating transformer.

Two connections will be considered. These essentially are the configuration shown by Figure 3.3 except that one of output terminals is grounded. The new connections are depicted by Figure 4.1.

A discussion of the analysis procedure for either connection is presented in Appendix B. The 5-turn prototype will be used to test these connections.

4.1 Unbalanced Transmission Line Parameters

There exist two transmission line modes for these connections. These are known in the literature as the balanced and unbalanced propagation modes [12]. For either the static or rotating transformer the unbalanced mode is undesirable. Measurements indicate that the parasitic effects of core loss, shunt capacitance-to-ground, and magnetizing reactance are a manifestation of the unbalanced-mode fields. On the other hand, the balanced-mode fields are more tightly confined to the line and generally there is little power dissipation if the surrounding dielectric has a low loss.

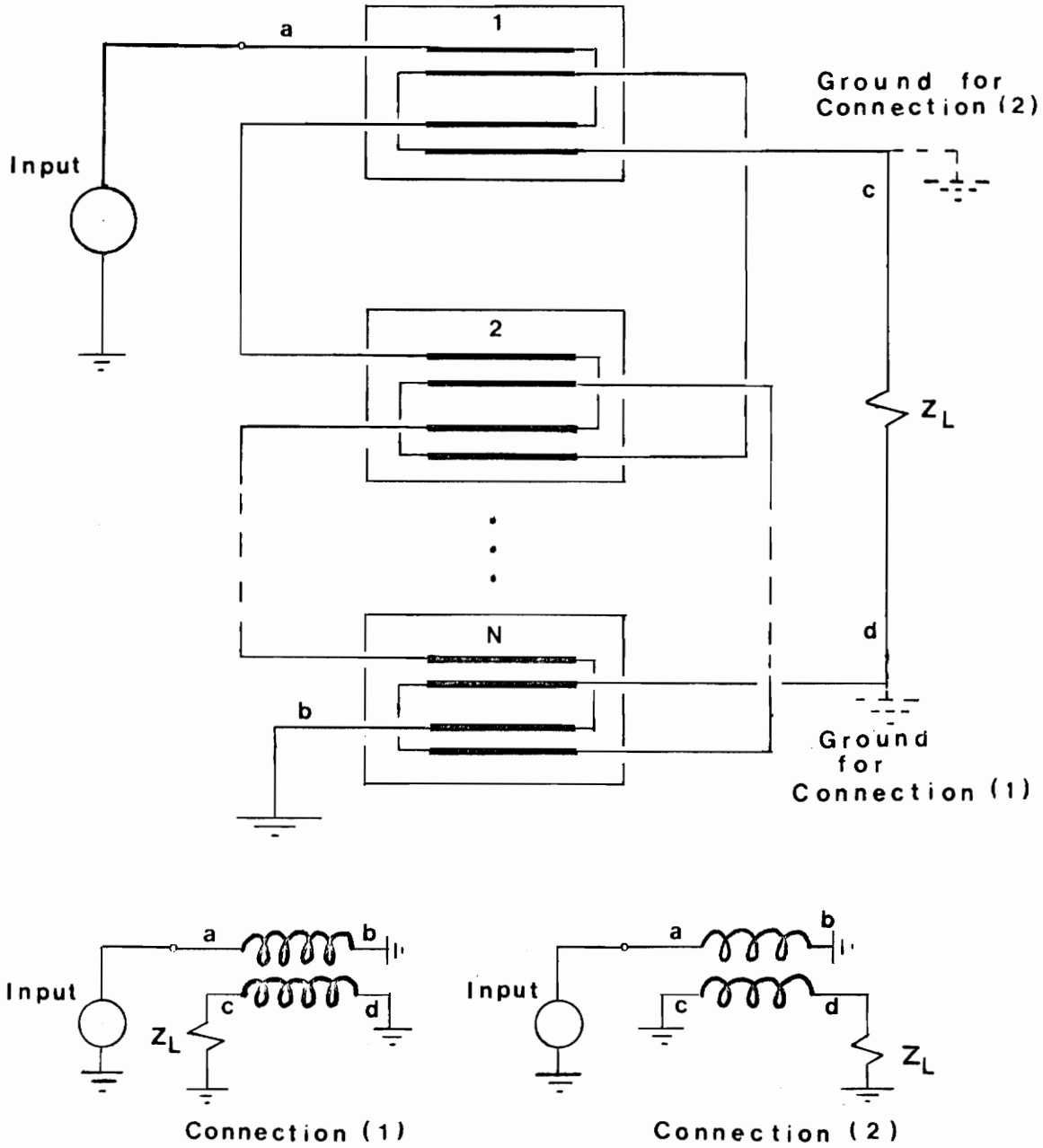

Figure 4.1 Two useful rotary transformer connections

A grounded metallic shield was placed around the prototype transformer. This was found necessary in order to facilitate the measurement of unbalanced-line parameters such as unbalanced characteristic impedance, Z_u, and the unbalanced propagation constant, γ_u. The measured values of the balanced-line parameters were unaffected by the shield. The balanced-mode parameters were discussed in Chapter III. The unbounded nature of the unbalanced-mode fields, however, will cause measurement fluctuation if the position of an unshielded transformer is altered relative to a ground plane. The shielding, while necessary for measurements, also simulates anti-crosstalk measures that must be taken if the rotary transformer is to be used for a stacked configuration or for multi-channel use.

The balanced line parameters, Z_o and $\beta\ell_T$ have been given. Also,

$$\alpha\ell_T \simeq 0 \tag{4.1}$$

since α is small and ℓ_T is short, the prototype is lossless in the balanced mode.

The unbalanced mode which propagates on the transmission line of the rotary transformer has been determined by measurement to be dispersive. Using the short circuit and open circuit measurement techniques outlined in Appendix B, the unbalanced parameters were determined for the prototype rotary transformer. The $\beta_u\ell_T$ product, illustrated by Figure 4.2.a., has a nonlinear variation with frequency. The $\alpha_u\ell_T$ product is not zero and is shown in Figure 4.2.b. The unbalanced characteristic impedance Z_u, has a complex value at high

frequencies. It is depicted by Figure 4.3. Each of these parameters display the properties common to a lossy transmission line mode.

A core air gap between the stator and rotor is a requirement if the transformer is to rotate freely. The air gap is formed between the two halves of the pot core used for the prototype model. One half of the pot core will turn with the rotor while the other half is fixed to the stator. The air gap separates the pot core pieces.

The unbalanced transmission line parameters, Z_u, $\alpha_u \ell_T$, and $\beta_u \ell_T$, obtained for several different air gap sizes are also shown in Figures 4.2 and 4.3. The parameters were determined from short circuit and open circuit measurements performed on the prototype transformer. A plastic shim was used to maintain air gap separation during experimentation.

The most extensive effect of an air gap is observed with $|Z_u|$ which fell from a value of 2000 ohms for no gap to approximately 600 ohms for a 12-mil air gap. To a good approximation the effects of an air gap on Z_u are directly related to the effects of air gaps on the inductance index, A_L. For any two different air gap sizes

$$\frac{|Z_{u1}|}{|Z_{u2}|} \cong \frac{A_{L1}}{A_{L2}} \tag{4.2}$$

Equation (4.2) is an empirical observation which is accurate at low frequencies. Errors in (4.2) occur at high frequencies because Z_u is related to distributed-line capacitance to ground [12].

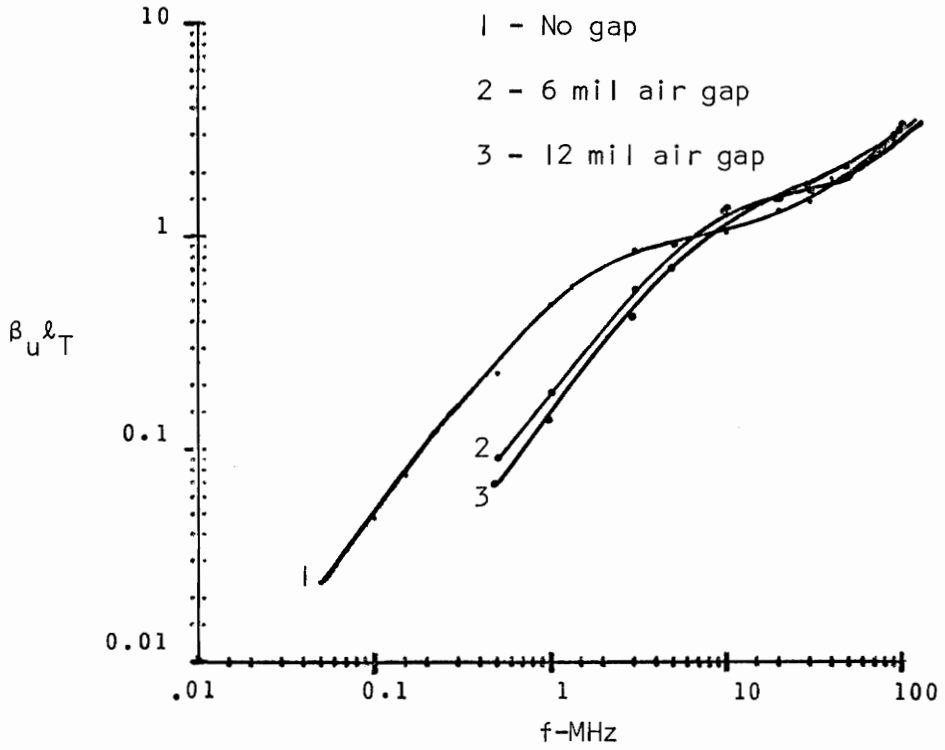

Figure 4.2.a $\beta_u \ell_T$ versus frequency

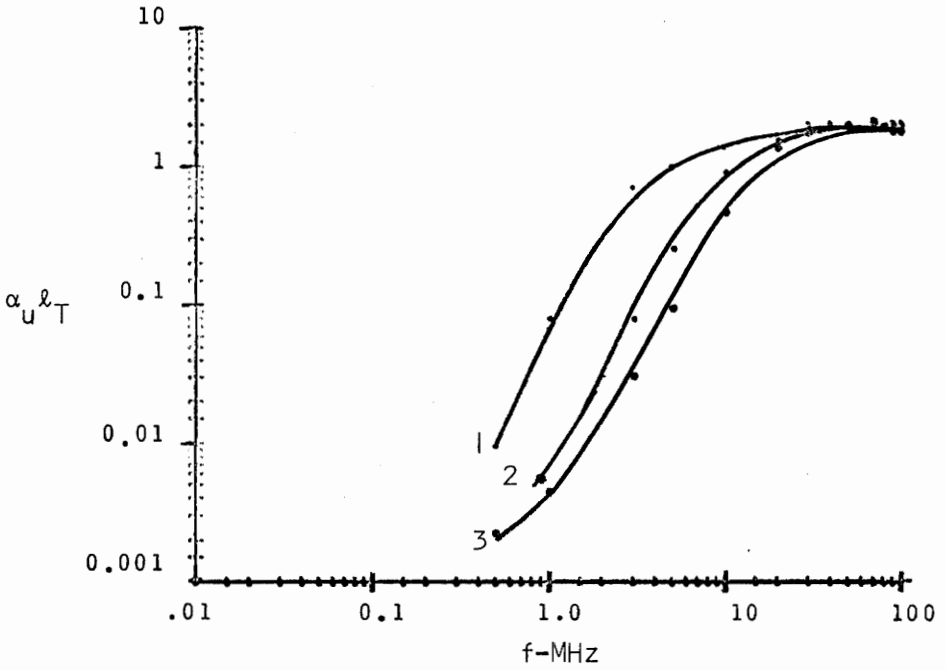

Figure 4.2.b $\alpha_u \ell_T$ versus frequency

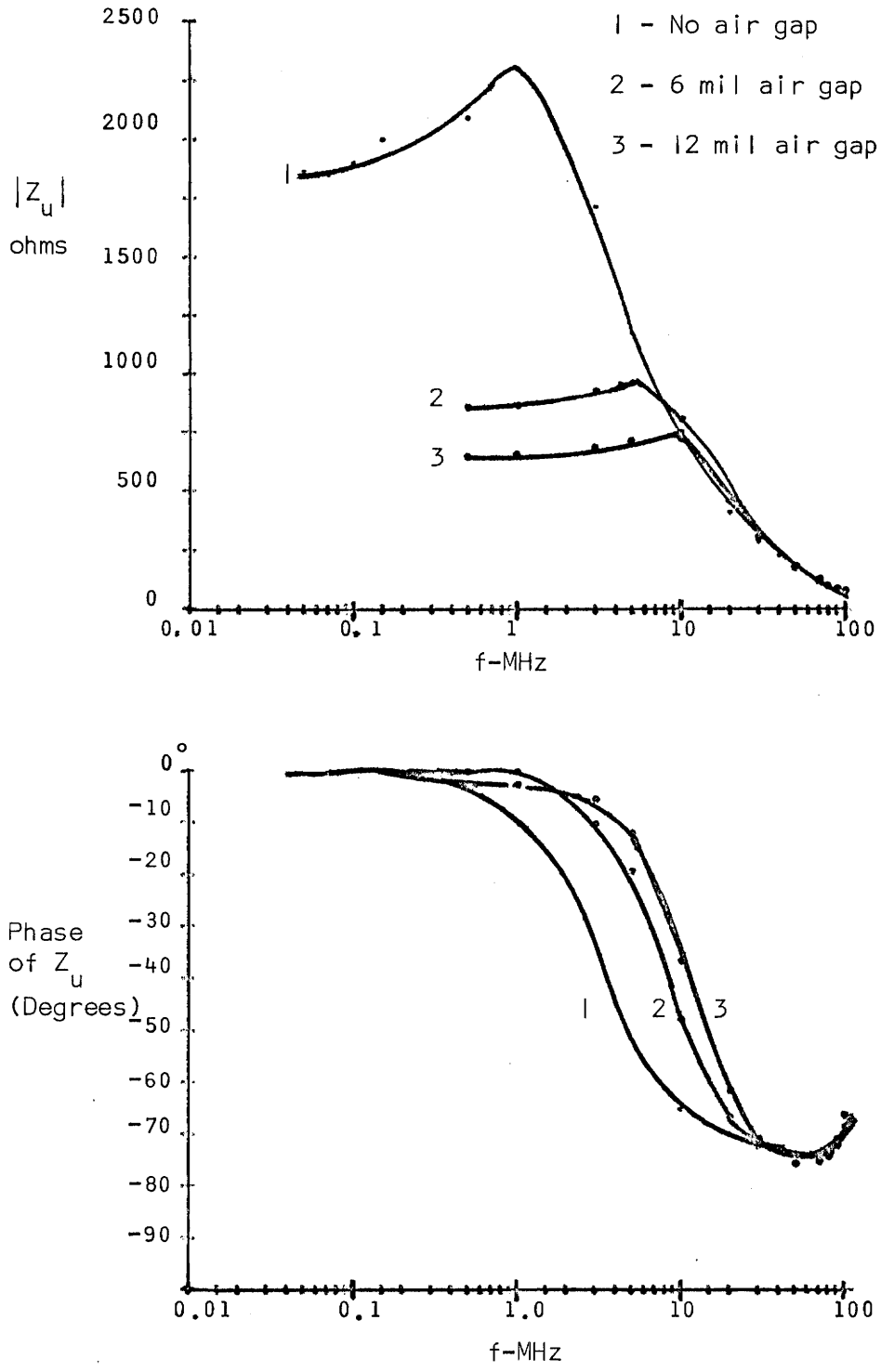

Figure 4.3 Unbalanced characteristic impedance

It is also interesting to note that the unbalanced mode propagates at a lower phase velocity than does the balanced mode. At low frequencies when both modes have low loss,

$$\frac{V_p}{V_u} = \frac{\beta_u}{\beta} \tag{4.3}$$

where V_p = balanced-mode phase velocity

V_u = unbalanced-mode phase velocity

Measurements with different air gaps indicate that as the air gap is increased, A_L, $|Z_u|$ and V_p/V_u decrease in magnitude but maintain their values to higher frequencies as shown by the tabulation:

$f < 1$ MHz, No gap: $A_L = 5500$, $|Z_u| \cong 2100$, $\frac{V_p}{V_u} = 25$

$f < 5$ MHz, 6-mil. gap $A_L = 1000$, $|Z_u| \cong 850$, $\frac{V_p}{V_u} = 10$

$f < 10$ MHz, 12-mil. gap: $A_L = 590$, $|Z_u| \cong 650$, $\frac{V_p}{V_u} = 7$

The transformer lower cutoff frequency can be expected to increase with air gap size. Equation (2.9), is useful for a determination of the lower cutoff. Due to a reduction of core flux because of air gap reluctance there is a reduction in core losses. As a result, there is a reduction in $\alpha_u \ell_T$. Also the unbalanced characteristic impedance, although reduced, tends to be real valued for slightly higher frequencies than observed with no air gap. Little change in transformer performance due to an air gap is expected at very high frequencies since the curves of Figures 4.2 and 4.3 converge for different air gaps.

4.2 Two Transformer Connections

The two networks depicted by Figure 4.1, are useful if there is a need for a common ground connection between the stator and rotor circuits. With the exception of rotation, these are 1:1 balun type connections. A computer analysis based on the discussion in Appendix B provides a comparison between predicted and experimental characteristics of the rotary transformer for these circuits.

These two configurations, hereafter designated as connection 1 and 2, were terminated with $Z_L = Z_0$ and will be examined for:

1) Variation of Input Impedance vs. Frequency
2) Insertion Loss Bandwidth
3) Power Transfer
4) Effects of Rotation (valid for 0-12 mil air gap)

4.3 Connection 1 (Figure 4.1) Response

The response curves for this connection are as follows:

1) Insertion Loss and Power Transfer: Figures 4.4, 4.5, and 4.6
2) Input Impedance: Figure 4.7, 4.8, and 4.9
3) Effects of Rotation on Input Impedance and Insertion Loss: Figures 4.10, 4.11, and 4.12

Note that experimental data as well as theoretical data are plotted. The measured 3 dB bandwidth of the transformer with no air gap is 80 kHz to 80 MHz (see Figure 4.4.a). With an increase of gap size the high frequency response is not affected. This is expected due to the transmission line parameter convergence noted at high frequencies (see Figure 4.2 and 4.3). However, the lower cutoff frequency is increased

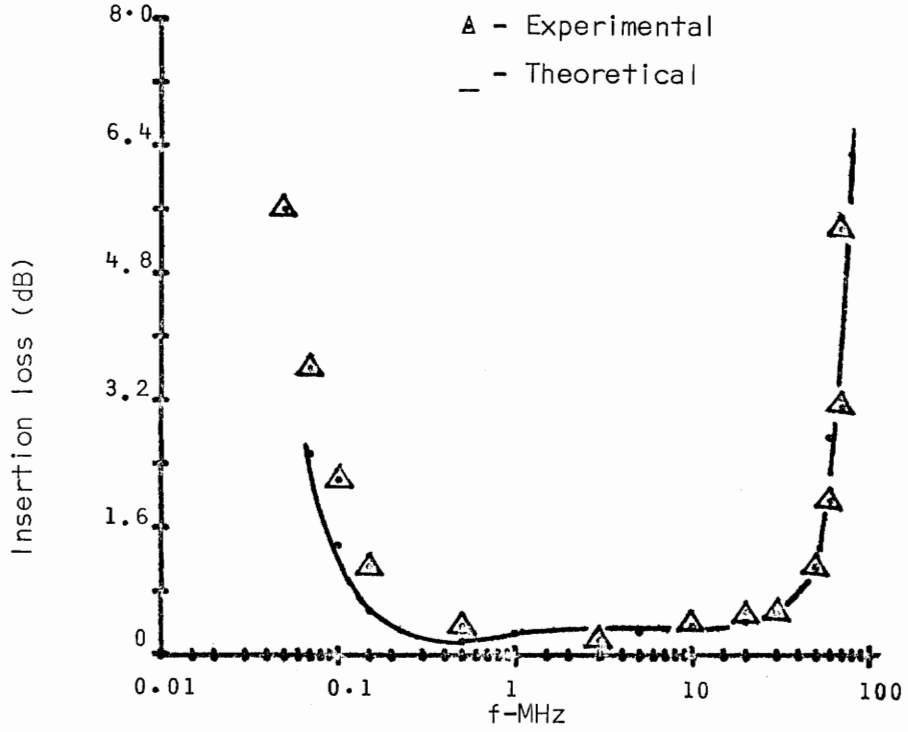

Figure 4.4.a Insertion loss (connection I, no air gap)

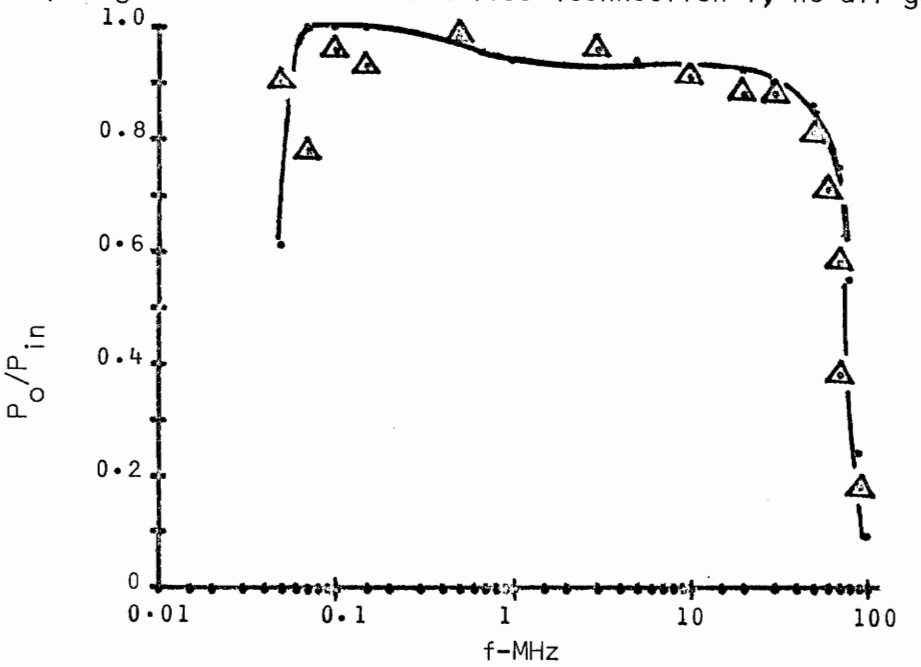

Figure 4.4.b Ratio of P_o/P_{in} (connection I, no air gap)

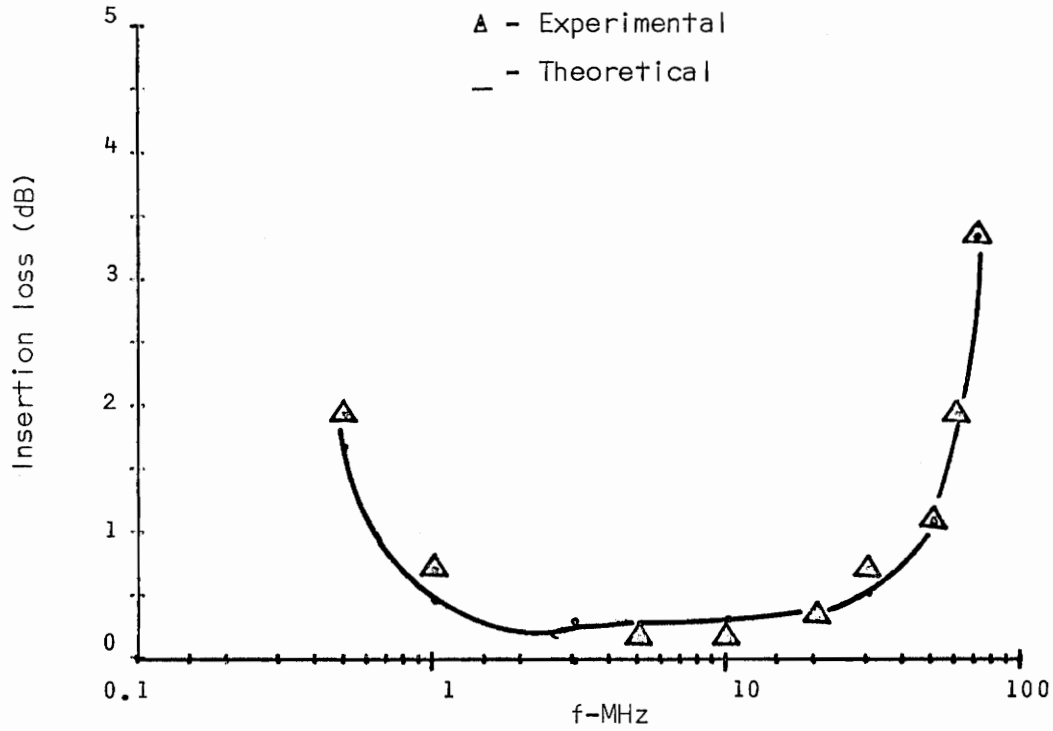

Figure 4.5.a Insertion loss (connection I, 6-mil air gap)

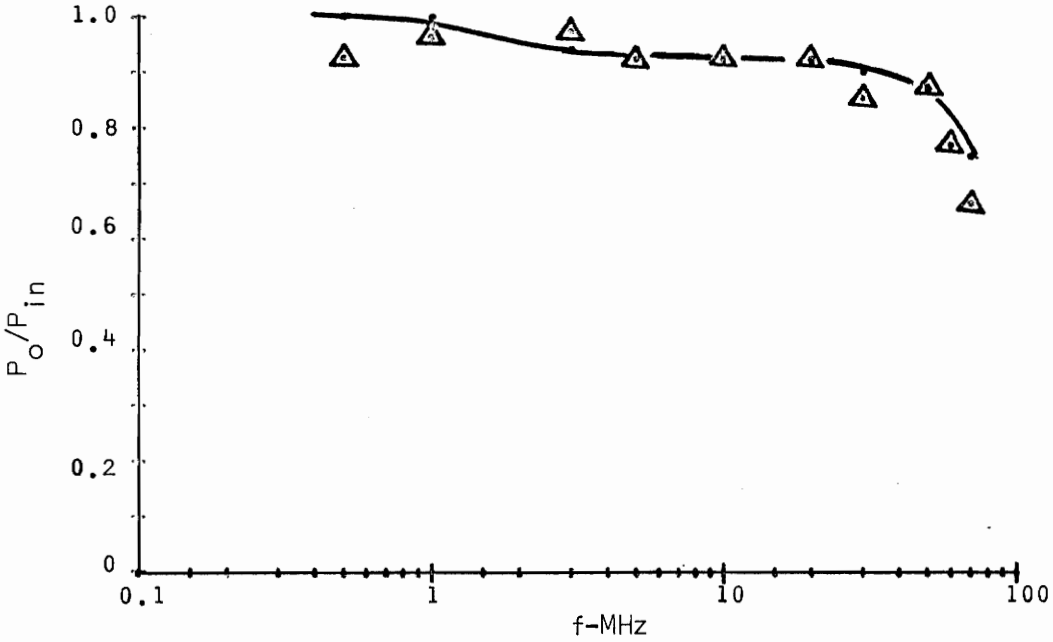

Figure 4.5.b P_o/P_{in} (connection I, 6-mil air gap)

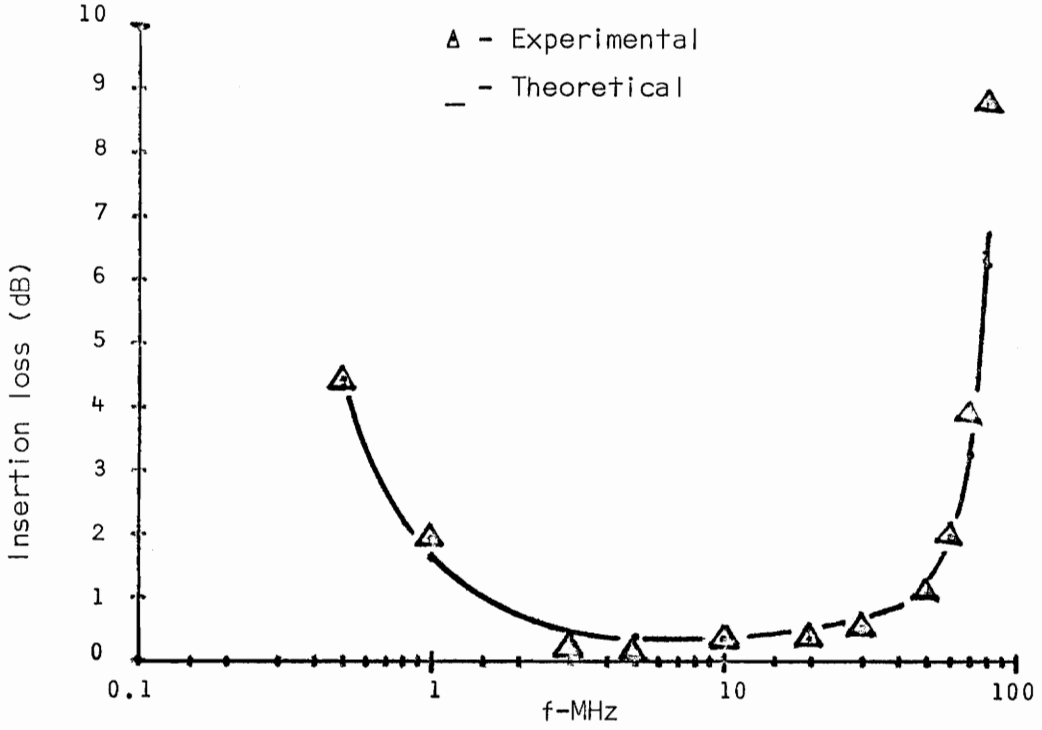

Figure 4.6.a Insertion loss (connection I, 12-mil air gap)

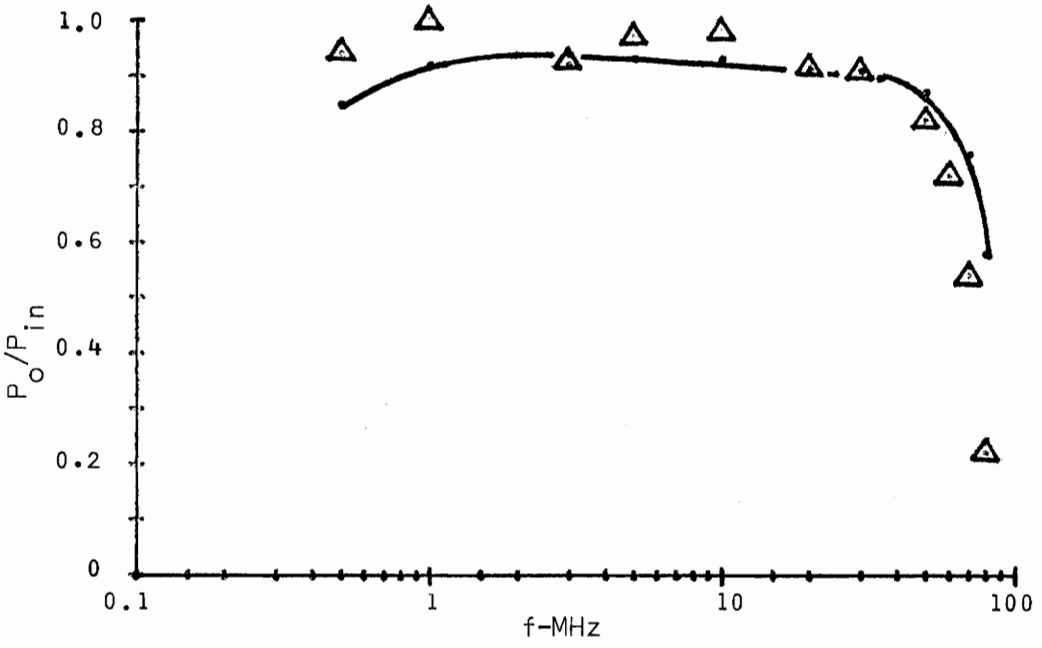

Figure 4.6.b P_o/P_{in} (connection I, 12-mil air gap)

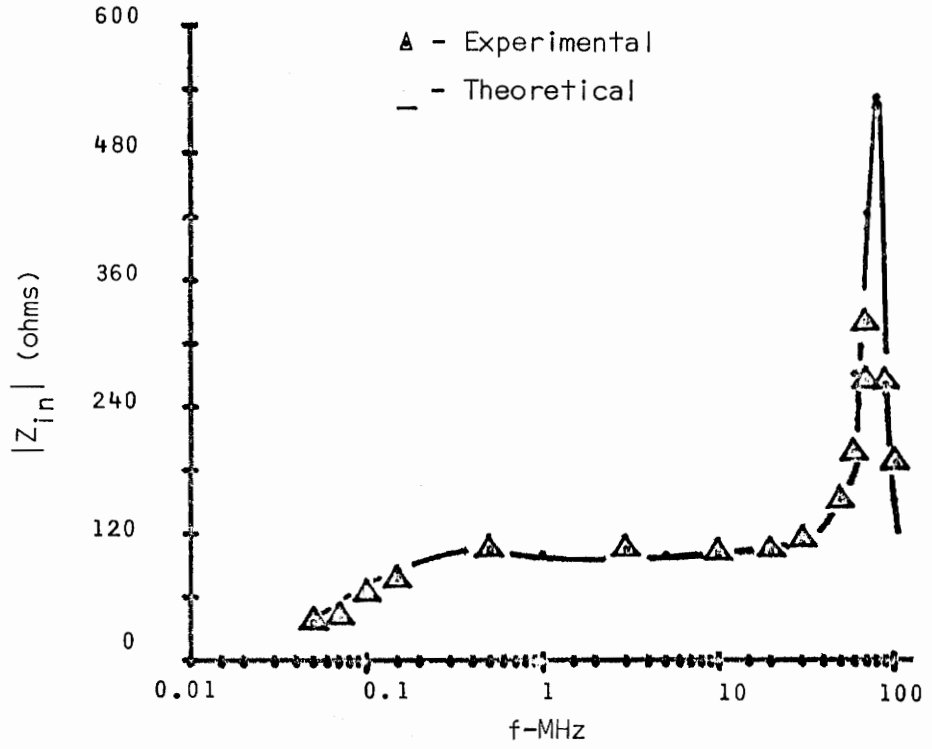

Figure 4.7.a Input impedance magnitude (connection 1, no gap)

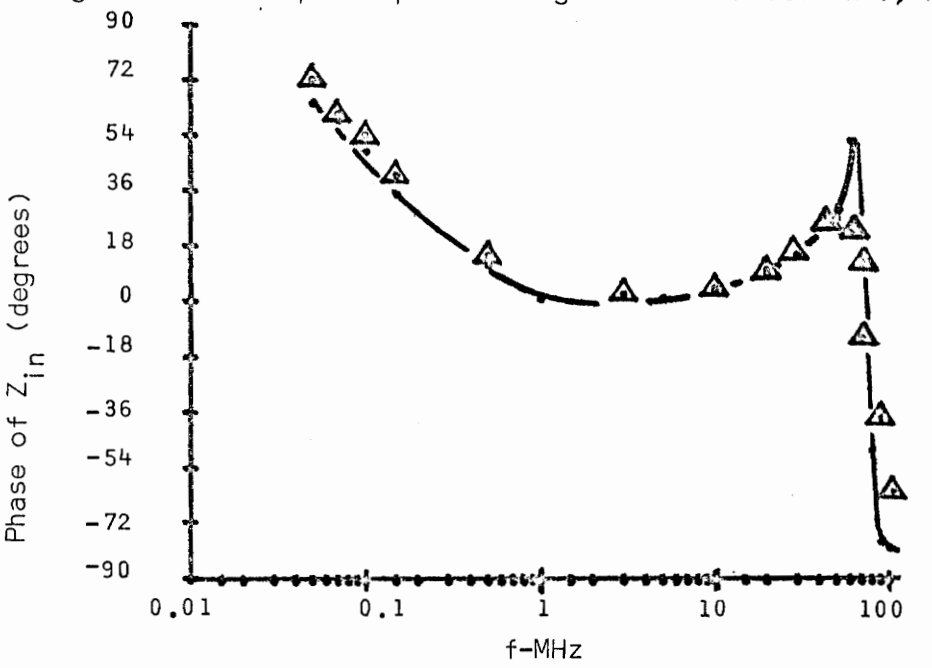

Figure 4.7.b Input Impedance Phase (connection 1, no gap)

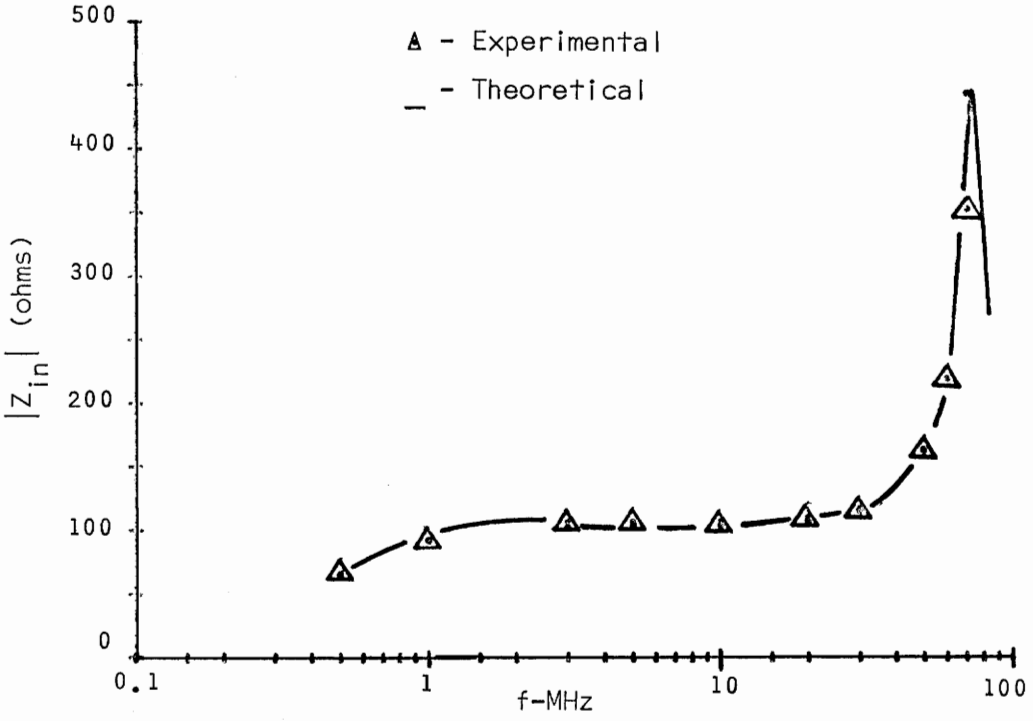

Figure 4.8.a Input impedance magnitude (connection 1, 6-mil gap)

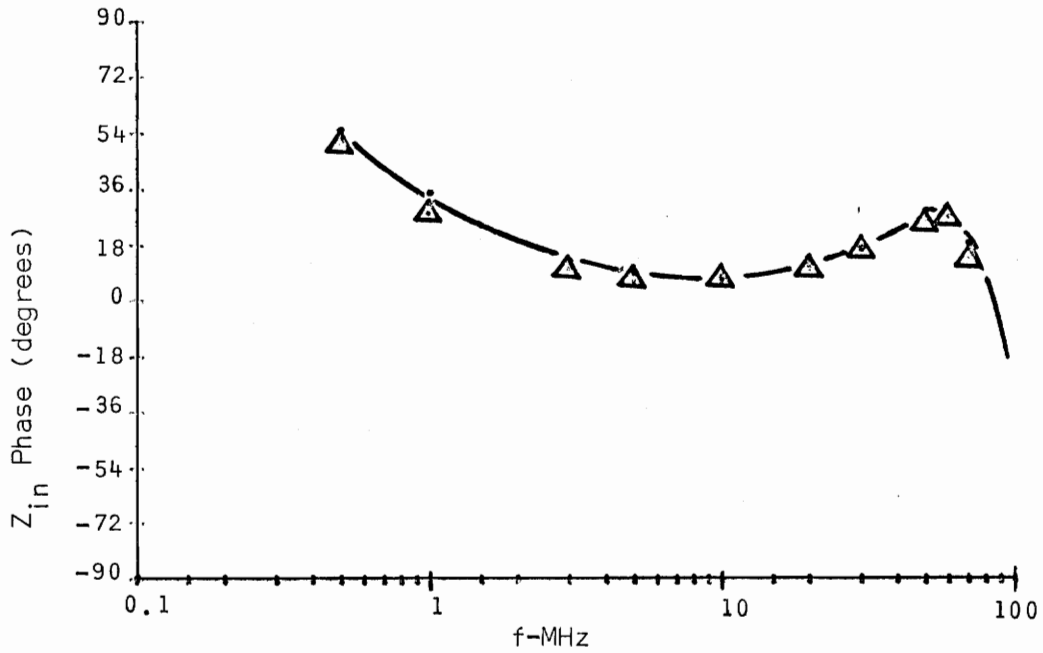

Figure 4.8.b Input impedance phase (connection 1, 6-mil gap)

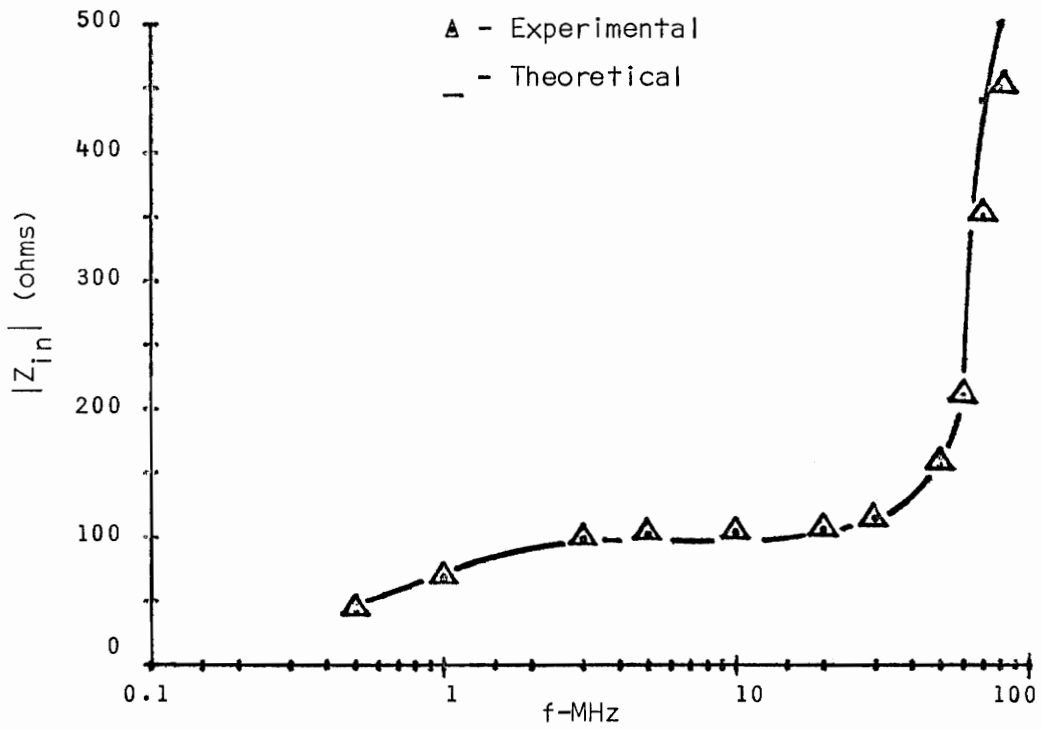

Figure 4.9.a Input impedance magnitude (connection 1, 12-mil gap)

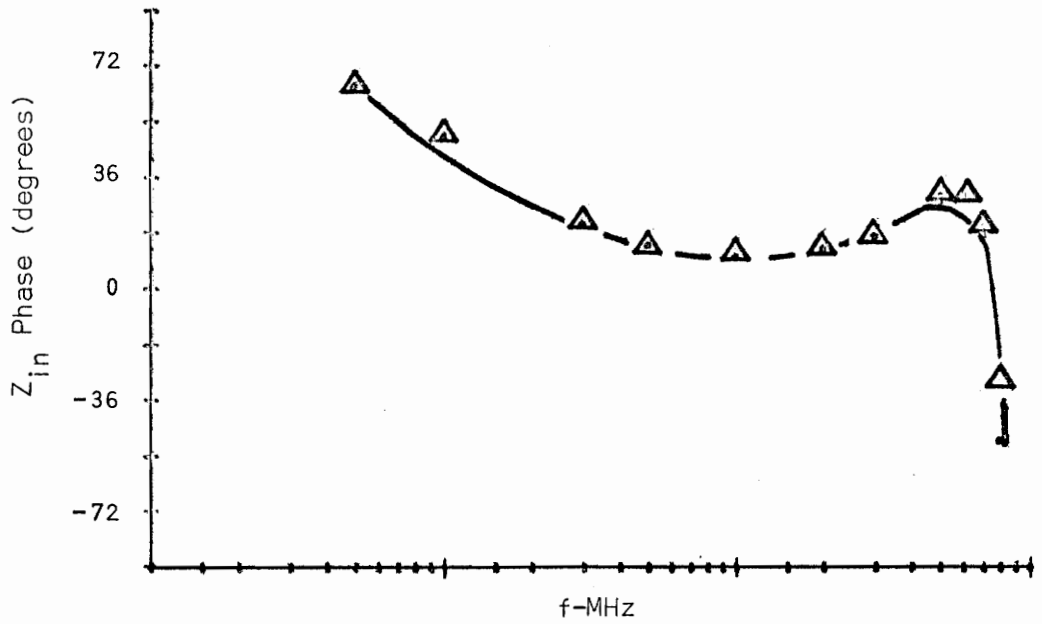

Figure 4.9.b Input impedance phase (connection 1, 12-mil gap)

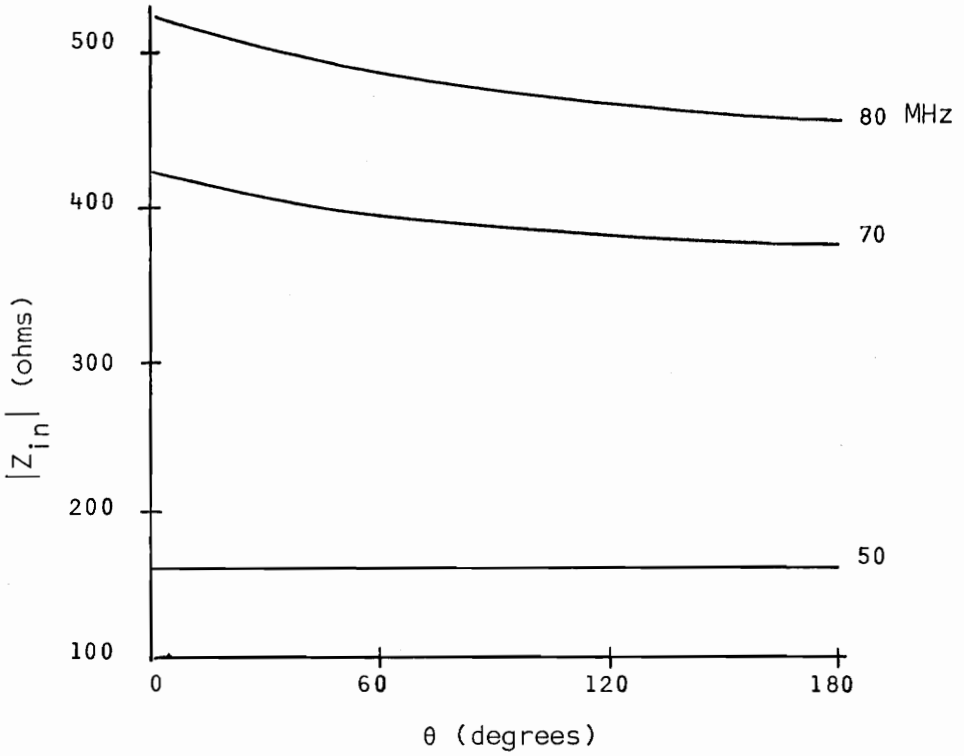

Figure 4.10.a Theoretical input impedance magnitude vs. rotation (connection I)

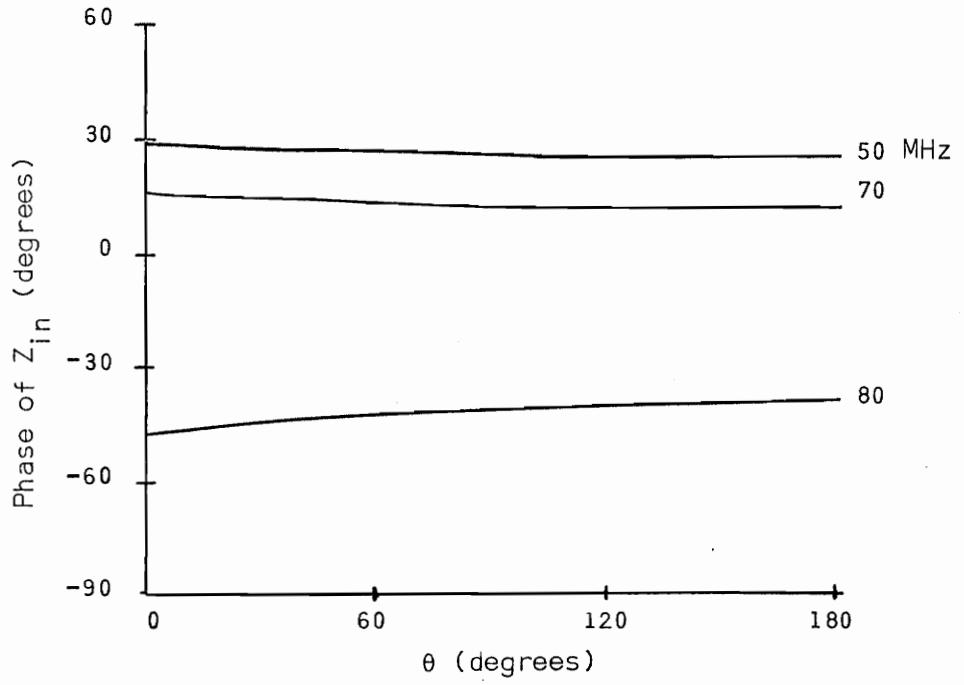

Figure 4.10.b Theoretical input impedance phase vs. rotation (connection I)

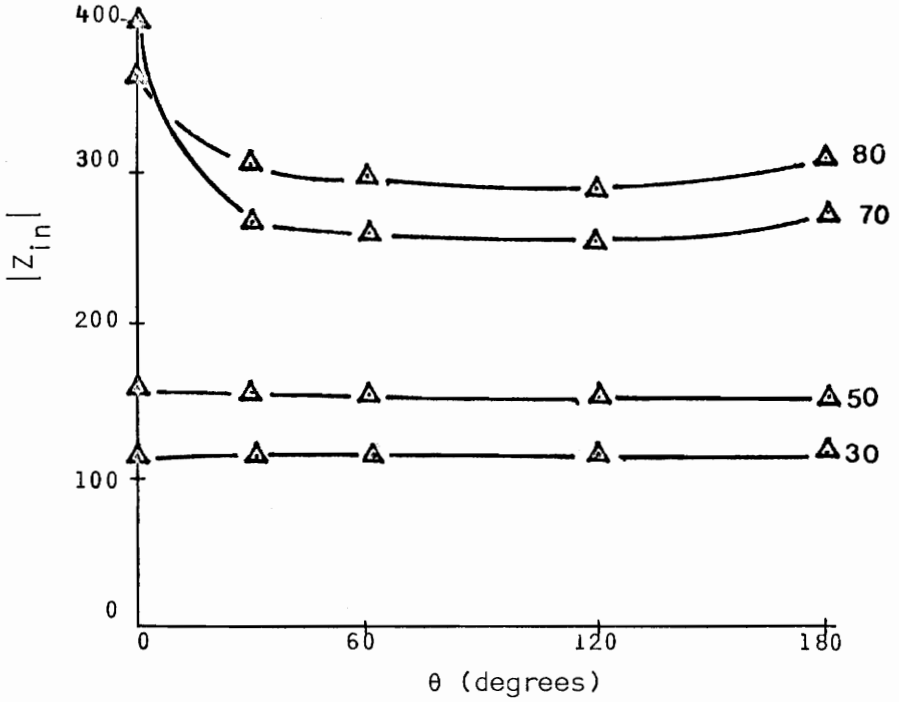

Figure 4.11.a Experimental input impedance magnitude vs. rotation (connection I)

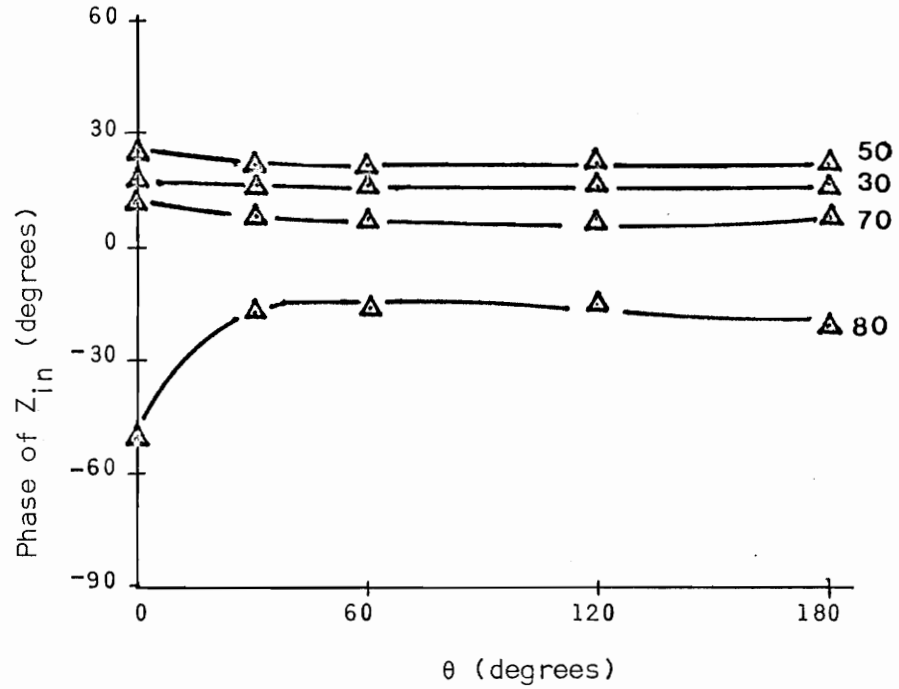

Figure 4.11.b Experimental input impedance phase vs. rotation (connection I)

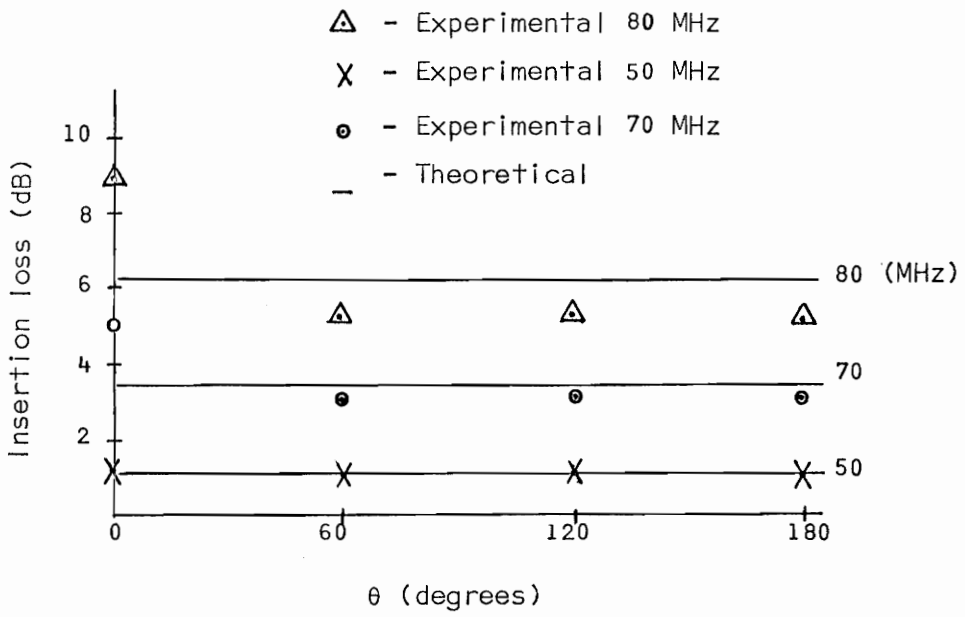

Figure 4.12 Insertion loss vs. rotation (connection 1)

to approximately 300 kHz with a 6 mil air gap, and to 500 kHz with a 12 mil gap (see also Figures 4.5 and 4.6). The power transfer curves (Figures 4.4.b, 4.5.b, and 4.6.b) relate the input terminal power, P_{in}, to the power absorbed by the load. The fraction of input power lost in the transformer can be determined from

$$\frac{P_{loss}}{P_{in}} = 1.0 - P_o/P_{in} \tag{4.4}$$

The input impedance curves (Figures 4.7, 4.8, and 4.9) depict the presence of a strong resonance condition near the upper cutoff frequency. This condition is caused by current being reflected from the ground plane short at the line output terminals and adding out of phase with the input current to the transmission line. Little power transfer occurs for connection 1 when the line length, ℓ_T, approaches $\lambda/4$.

This resonance condition reduces the usefulness of this connection. Near resonance the device is sensitive to rotation. It is thought, too, that capacitance to ground between the input leads feeding the transformer rotor and stator aggravate the sensitivity of the transformer to rotation. Note in Figure 3.2 how the connections are brought out from the top of the stator or rotor coils. In order to connect to the opposite coil end a short length of wire must pass longitudinally behind each winding. Changes in the transformer response occur at $\theta = 0°$ when these wires connected to the rotor and stator coils align (see Figures 4.11 and 4.12). This effect is not observed when the line length is $\ell_T \leq \lambda/8$, approximately at 40 MHz for this transformer. Also, when the shield is removed and connections discussed in Chapter III are used no such rotational sensitivity is observed.

4.4 Connection 2 (Figure 4.1) Response

The response curves for this connection are as follows:

1) Insertion Loss and Power Transfer: Figures 4.13, 4.14, and 4.15
2) Input Impedance: Figures 4.16, 4.17, and 4.18
3) Effects of rotation: Figures 4.19, 4.20, and 4.21

This connection exhibits a very good frequency response compared with that of connection 1. There is no strong resonance effect observed near cutoff, and the impedance match is flat for a wide range of frequencies. The low frequency response is typically the same as that observed with connection 1, but due to the lack of the resonance the upper cutoff frequency is enhanced by approximately five to ten megahertz.

Resonance is not a problem with this connection due to the placement of the load impedance. For this configuration, little power is reflected from the matched load impedance, $Z_L = Z_0$, terminating the transmission line output.

This balun type connection is a standard type used for static transformers [1, 13]. The rotating transformer performs well with this connection also. The absence of resonance reduces the sensitivity of the transformer to rotation (see Figures 4.19, 4.20, and 4.21). Near the upper cutoff the effects introduced by the input leads are present but are not as pronounced as were observed for connection 1. If there is a common ground between rotor and stator circuits connection 2 should be used.

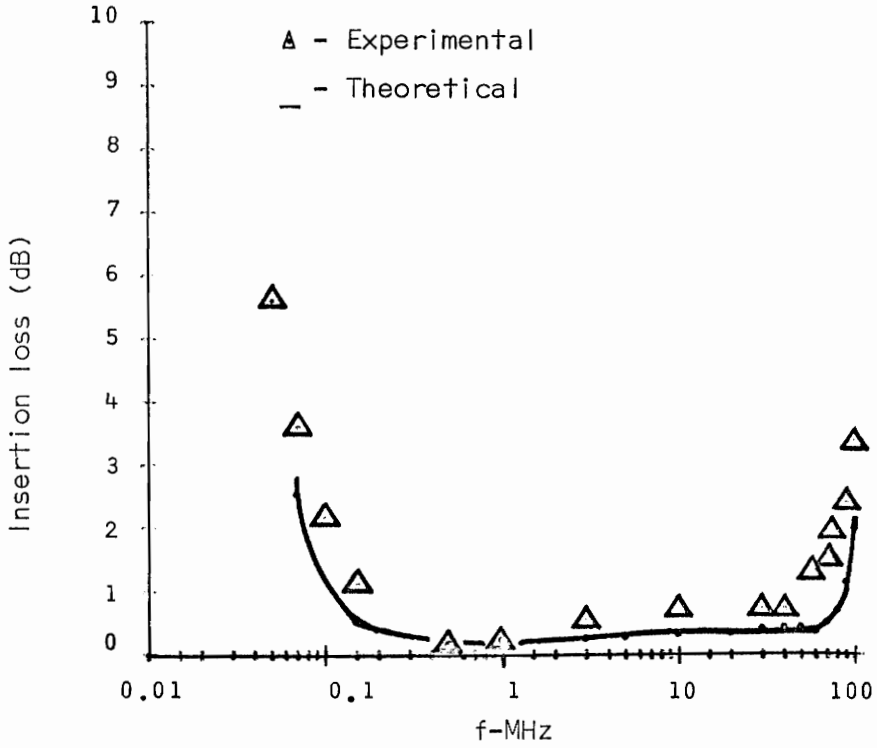

Figure 4.13.a Insertion loss (connection 2, no air gap)

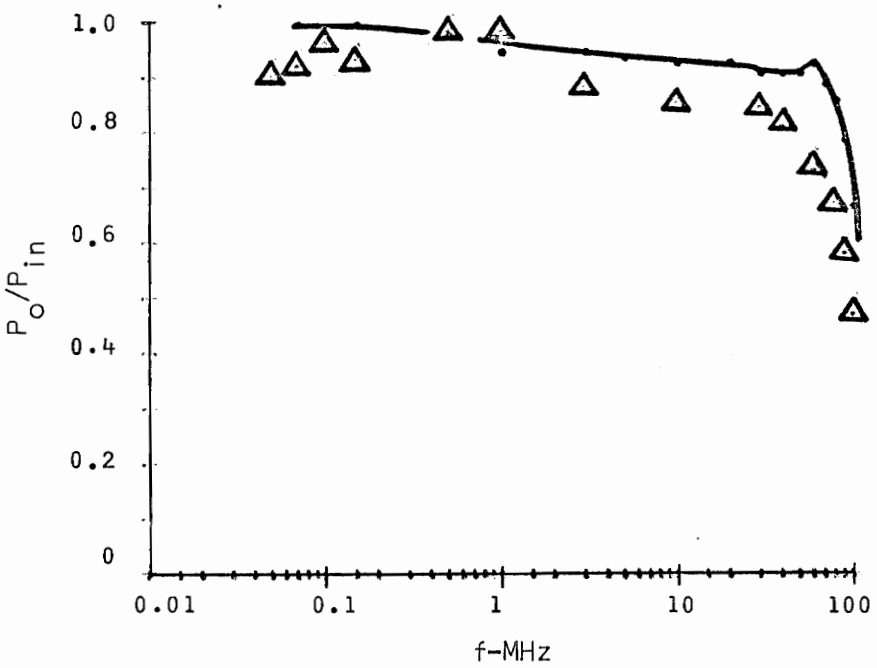

Figure 4.13.b P_o/P_{in} (connection 2, no gap)

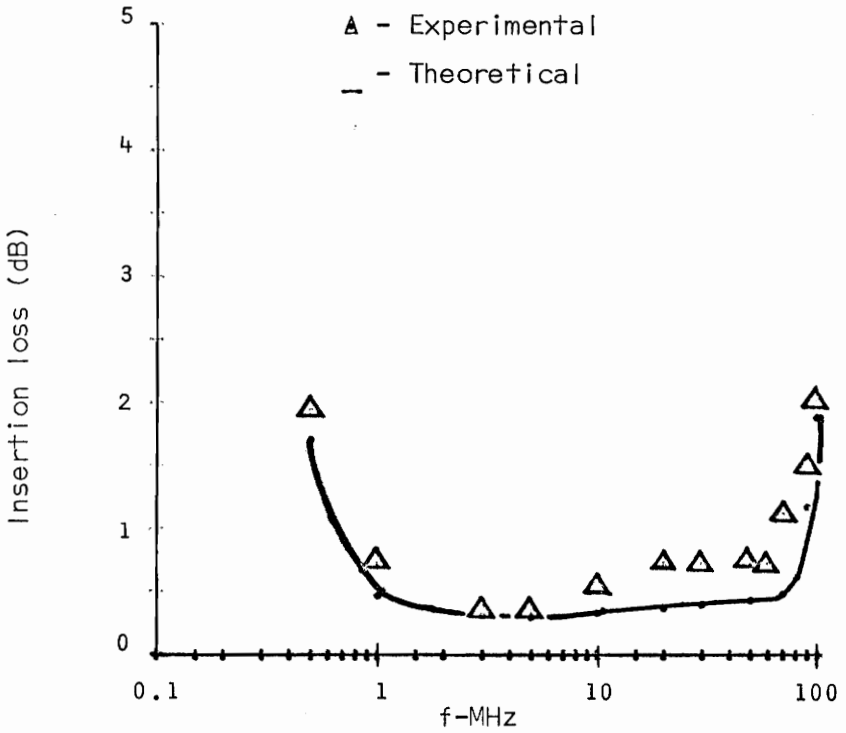

Figure 4.14.a Insertion loss (connection 2, 6-mil gap)

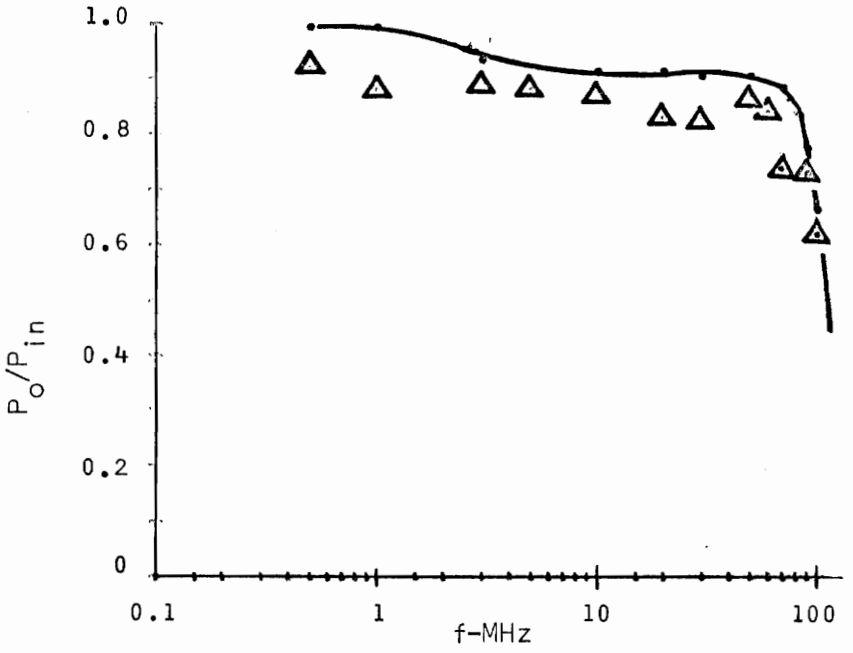

Figure 4.14.b P_o/P_{in} (connection 2, 6-mil gap)

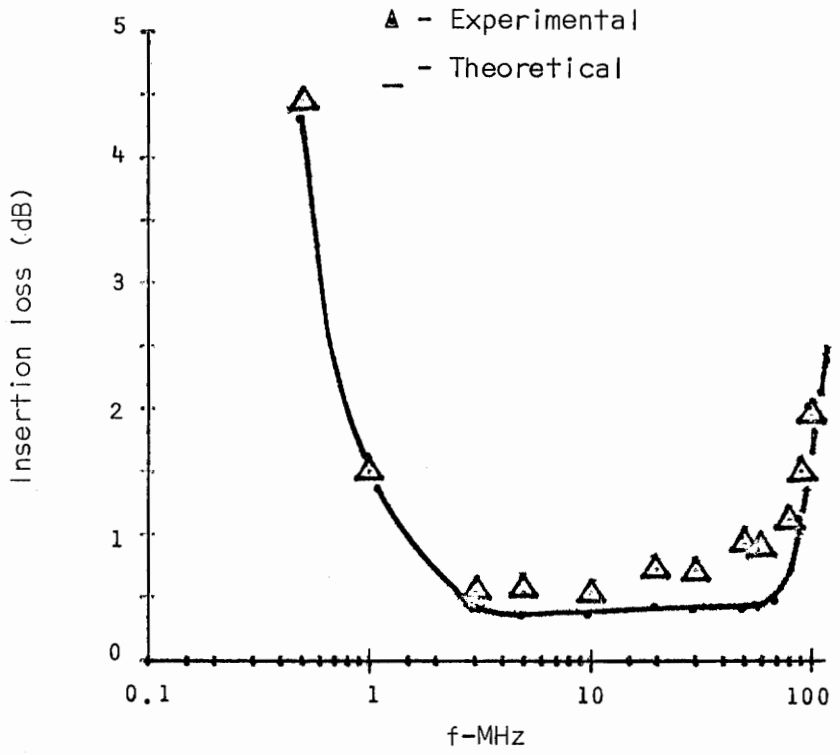

Figure 4.15.a Insertion loss (connection 2, 12-mil gap)

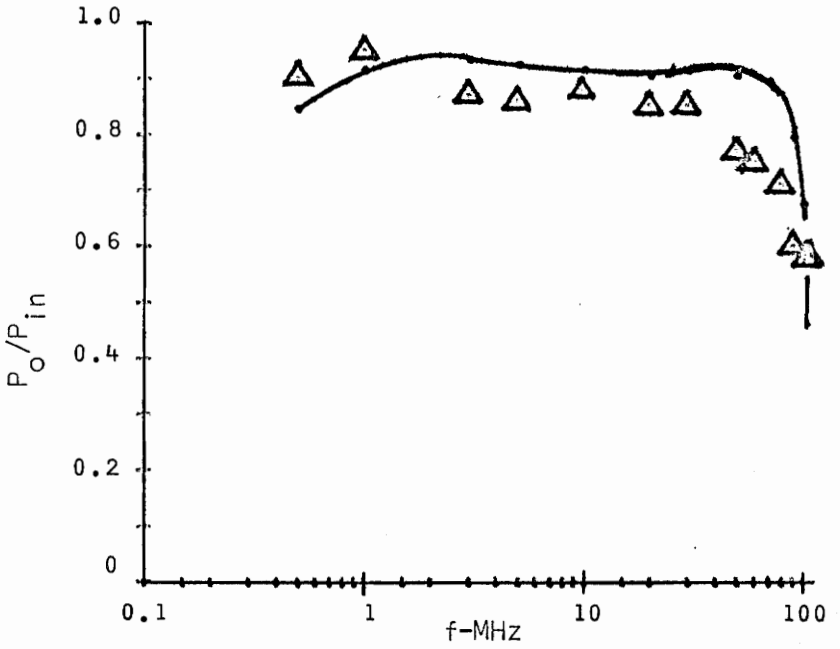

Figure 4.15.b P_o/P_{in} (connection 2, 12-mil gap)

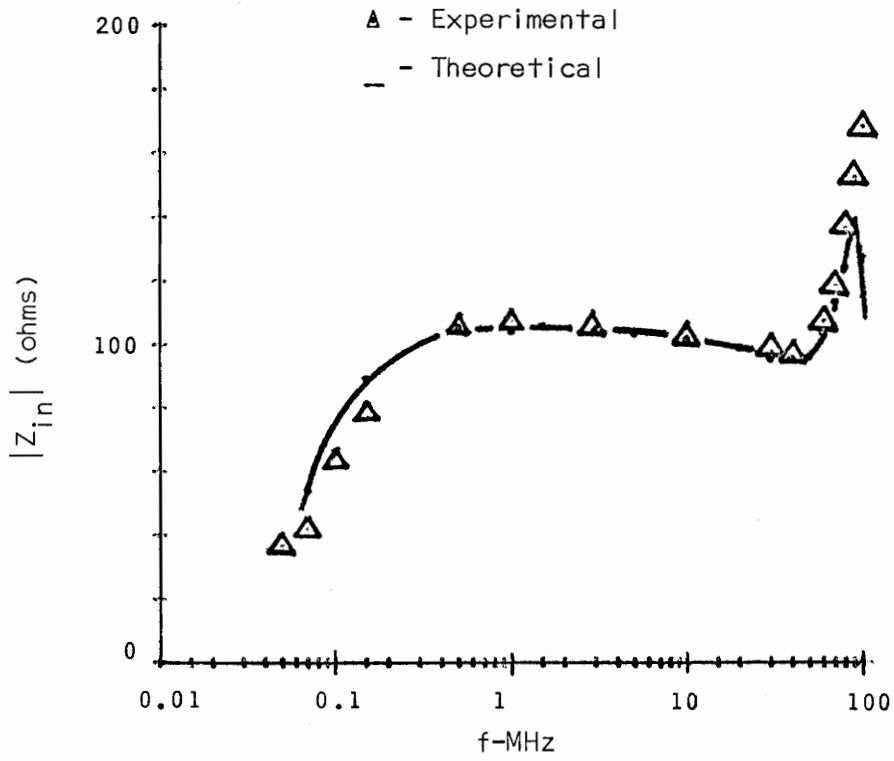

Figure 4.16.a Input impedance magnitude (connection 2, no gap)

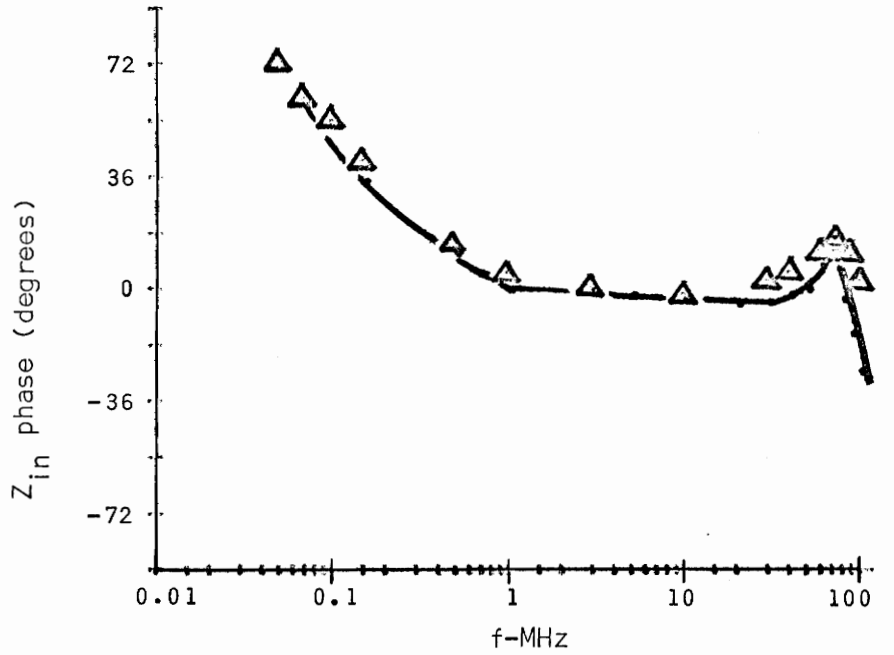

Figure 4.16.b Input impedance phase (connection 2, no gap)

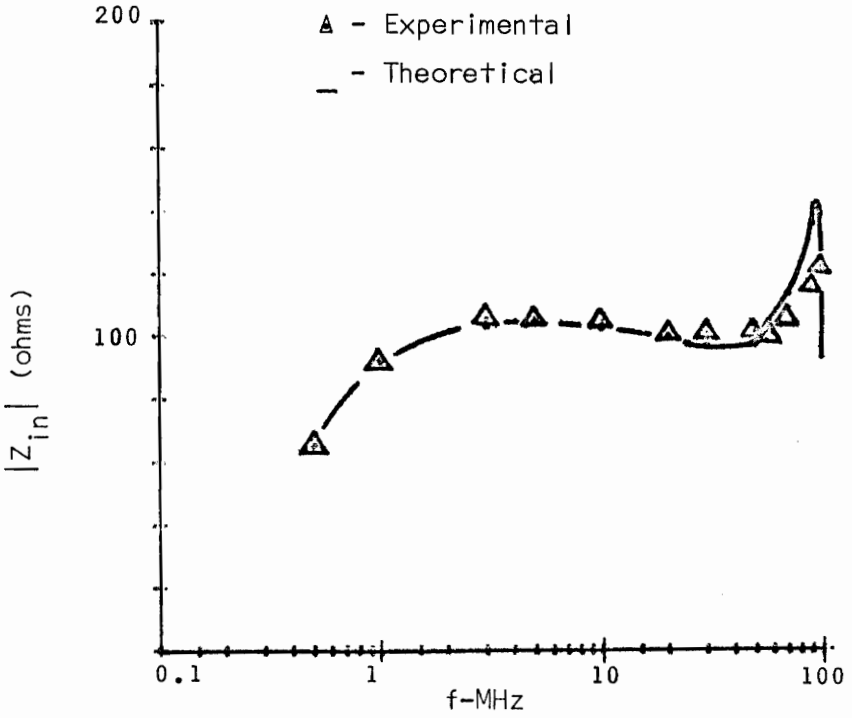

Figure 4.17.a Input impedance magnitude (connection 2, 6-mil gap)

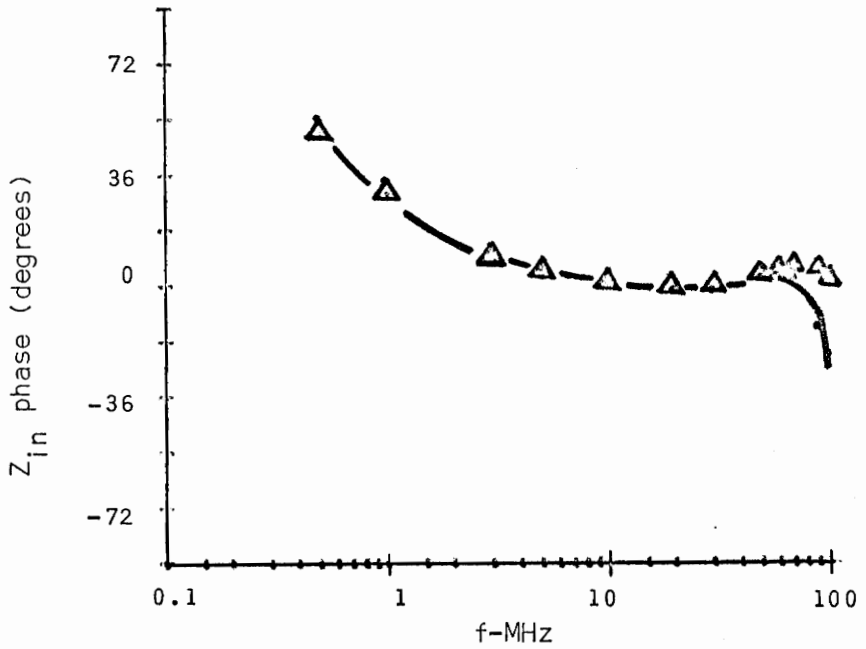

Figure 4.17.b Input impedance phase (connection 2, 6-mil gap)

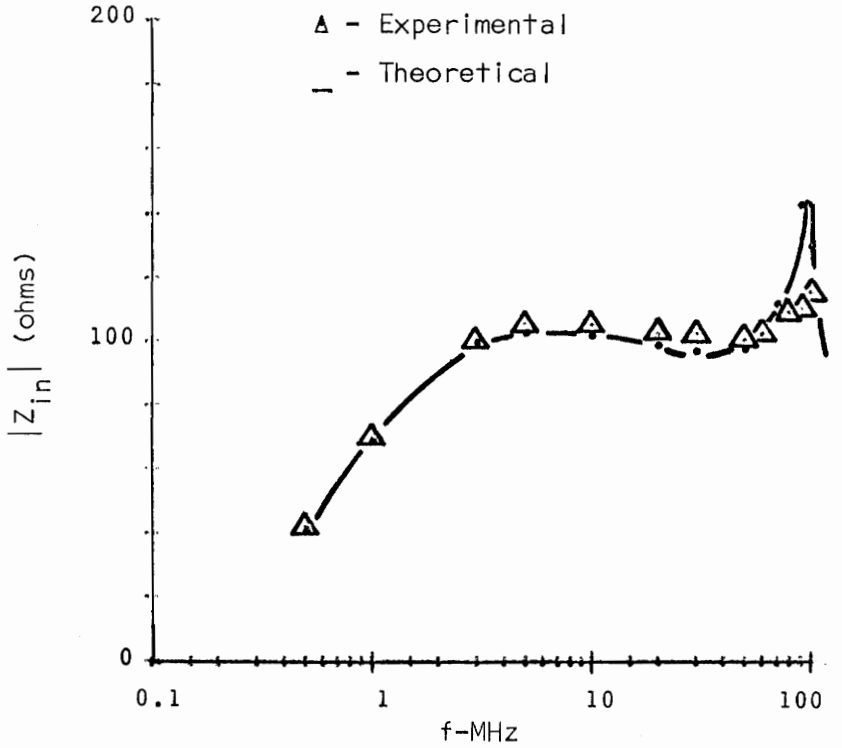

Figure 4.18.a Input impedance magnitude (connection 2, 12-mil gap)

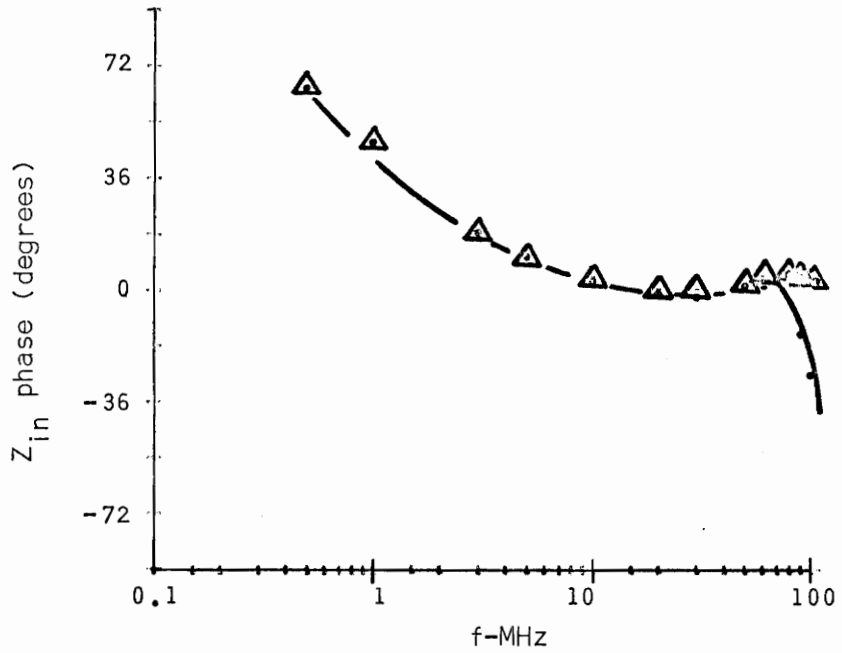

Figure 4.18.b Input impedance phase (connection 2, 12-mil gap)

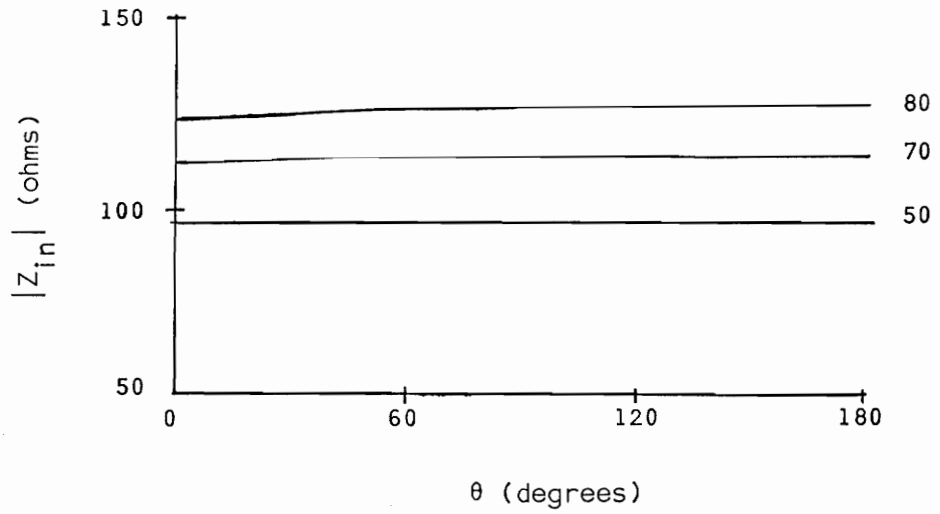

Figure 4.19.a Theoretical input impedance magnitude vs. rotation (connection 2)

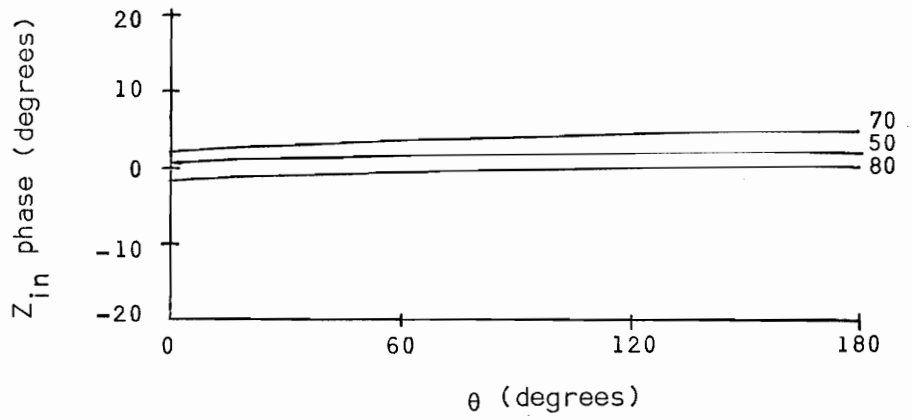

Figure 4.19.b Theoretical input impedance phase vs. rotation (connection 2)

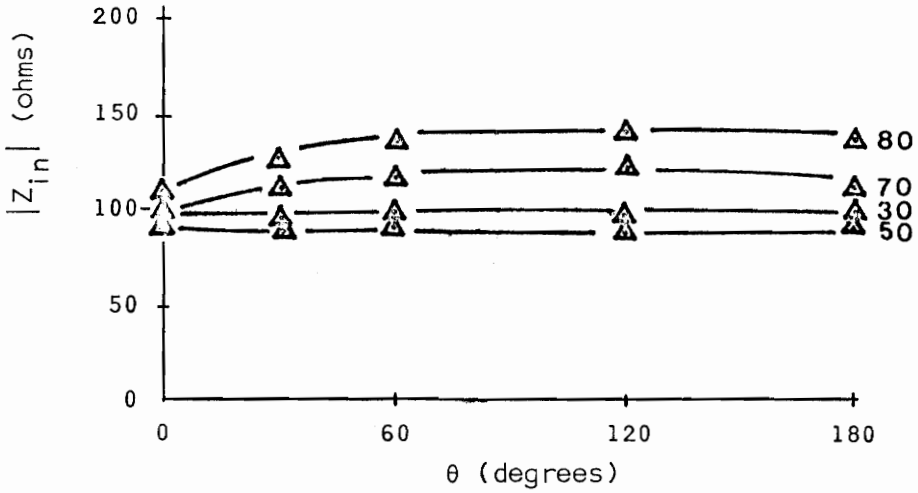

Figure 4.20.a Experimental input impedance magnitude vs. rotation (connection 2)

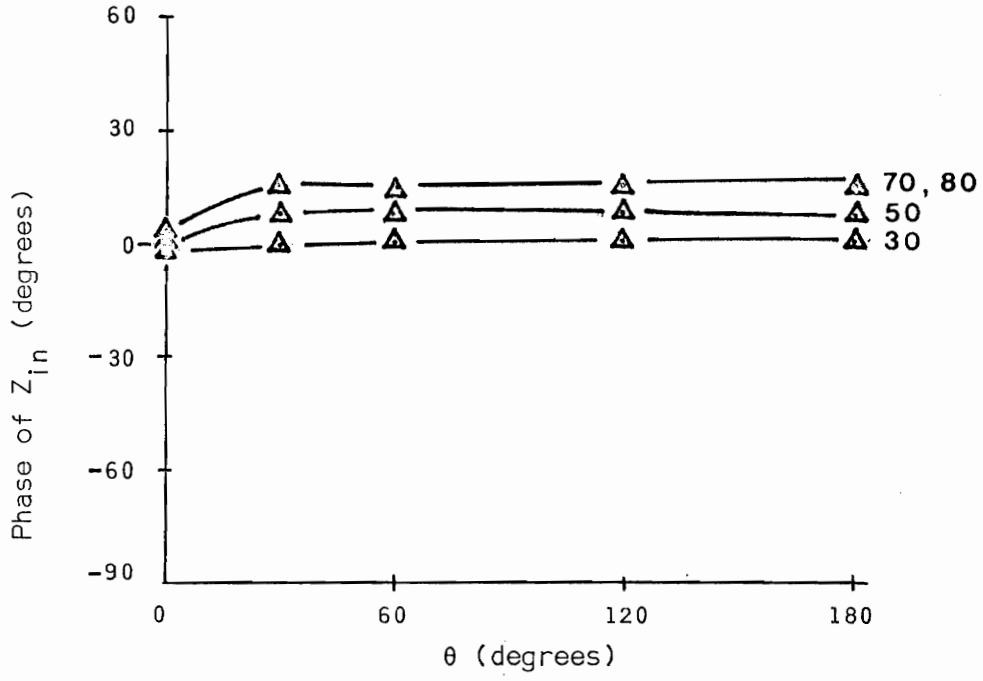

Figure 4.20.b Experimental input impedance phase vs. rotation (connection 2)

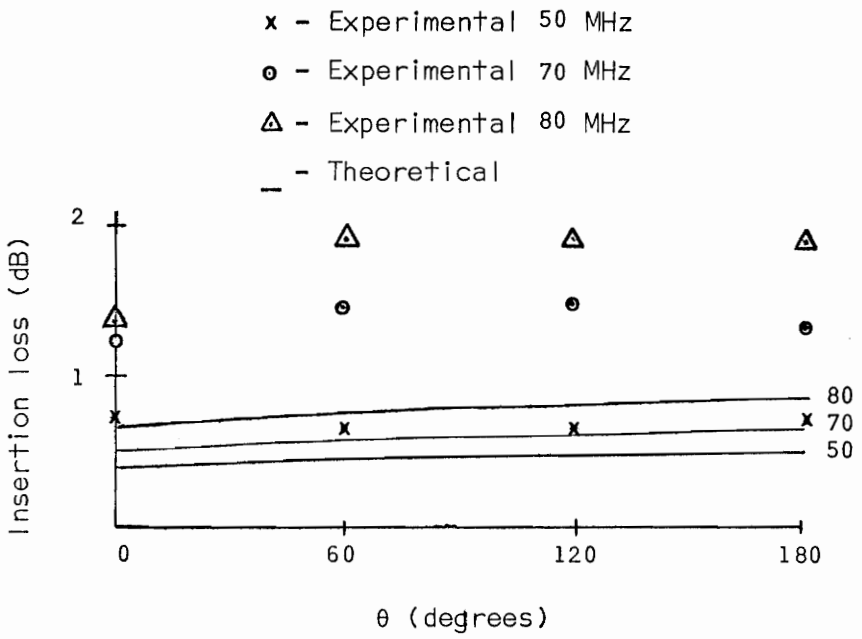

Figure 4.21 Insertion loss vs. rotation (connection 2)

V. CONCLUSIONS

5.1 Summary

The theory of static wideband transformers has been applied to the design of a VHF rotary coupler that has a bandwidth ratio of 1000:1, and that requires no physical contact between the stator and rotor. A combination of balanced and unbalanced transmission line theory has been used to predict the performance of the coupler, and measurements on the prototype model showed excellent agreement with predicted values. Input impedance and insertion loss were shown to be essentially independent of rotation over a wide frequency range.

A significant aspect of this work is the analysis of the rotating turn in terms of two transmission line segments of variable length. This, coupled with the unbalanced-line theory from Sato [12], led to a complex analysis that resulted in a system of 20 simultaneous equations to describe the 5-turn transformer. Thus, a computer solution was the only feasible method to predict the coupler performance.

The recommended circuit connections depend upon the application:

(1) If the rotor circuit can "float" off ground, and if no shielding is required, the circuit of Figure 3.3 is best.

(2) If an unbalanced load (one side grounded) is required, the connection of Figure 3.4.b gives the best performance except that the added balun (static transformer) will contribute an additional 0.5-1 dB of loss.

(3) The balun can be omitted by use of connection 2 in Figure 4.1. This connection is somewhat more sensitive to rotation than that of Figure 3.4.b.

When a shield is used to prevent crosstalk with other circuits, the performance of the coupler is affected slightly by its proximity to the shield, as shown by measurements of the unbalanced-line parameters.

An air gap is necessary between the two halves of the pot core in order to allow free rotation. Data taken with gaps from 0 to 12 mils indicate that the primary effect of a gap is to raise the lower cutoff frequency because of the decrease in primary inductance. High frequency performance was not affected by the presence of the air gap.

5.2 Possible Applications

The rotary coupler should find application wherever electrical signals above the audio range are to be transmitted between a stationary and a rotating structure, particularly if wide bandwidths are required. Slip rings are used for many such applications, but they produce electrical noise and may overheat at high speeds due to brush friction. The rotary coupler has no sliding contacts, and thus avoids these problems.

The device could be used as a coupler to continuously-rotating antennas, and also to television antennas to avoid problems with wrap-around cables. It would also be useful for telemetering experimental data from high-speed turbines or other rotating structures to a stationary terminal. One limitation on such applications should be

mentioned--the physical size (diameter) of the coupler must not be so large that the transmission-line wavelength will exceed 0.3λ at the highest frequency.

5.3 Suggestions for Further Research

(1) Because of equipment limitations, all measurements for this dissertation were made at a power level of less than 10 millwatts. As the transmitted power is increased, losses in the ferrite core would be expected to increase. The way in which core loss varies with power level and frequency should be investigated in order to establish some sort of power rating for a given size core and core material. This investigation would be equally valid for static transformers.

(2) The moving parts of the prototype rotary coupler (see Figure 3.2) consist of a nylon "sleeve bearing" in which the windings are embedded and the two halves of the pot core. For high-speed applications this configuration would not be desirable from a mechanical standpoint. It is suggested, therefore, that the configuration shown in Figure 5.1 be investigated. Here each winding is in one plane, either imbedded in or plated upon a ferrite disc. Each turn of a winding is circular, as shown in Figure 5.1, and the successive turns are series connected. If the turns placed upon the two discs are mirror images, they will form parallel-wire transmission lines whose (balanced) characteristic impedance is a function of the conductor width and spacing; hence the value of Z_o could be adjusted by the spacing between the stationary and rotating discs. The analysis used in this report should

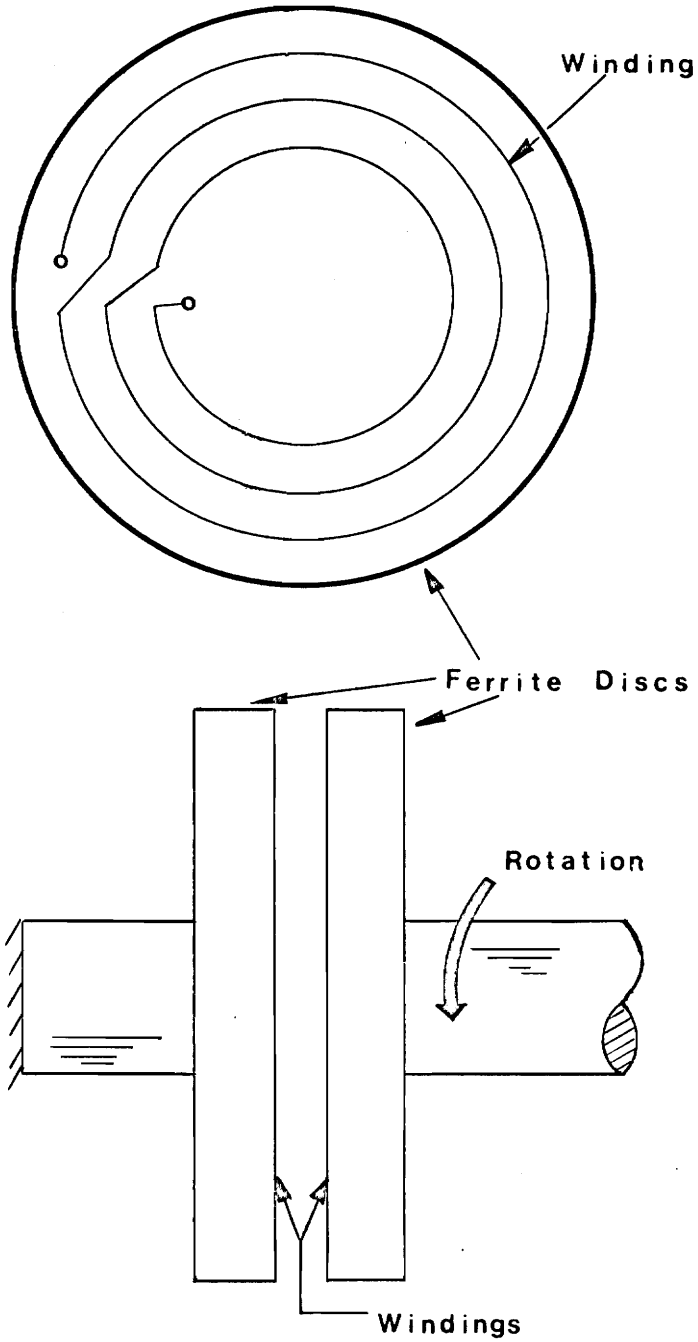

Figure 5.1 Planar rotary transformer

apply directly to this type of configuration, except that each turn will have a different total length.

(3) Manufacturer's data sheets on ferrite materials generally do not give information on initial permeability, inductance index, and loss tangent over the frequency range in which the cores are useful. Thus it is not possible to predict wideband performance of the transformer from catalog data.

The measurement of balanced and unbalanced line parameters to gain information for such predictions is time-consuming, and can be done only after the transformer is built. Construction and evaluation of a number of transformers using a variety of core materials might yield at least an empirical guide for preliminary design, or at best a means of improving data-sheet information.

The behavior of different types of ferrite core materials over wide frequency bands requires investigation, for it appears from the research reported here that these cores are useful to much higher frequencies than catalog information indicates.

APPENDIX A

Balanced Current Transmission Line Analysis

For a two-wire lossless transmission line in Figure A.1, two-port transmission equations are

$$\begin{bmatrix} V_S \\ I_S \end{bmatrix} = \begin{bmatrix} A & B \\ C & D \end{bmatrix} \cdot \begin{bmatrix} V_R \\ I_R \end{bmatrix}$$

$$\text{where } \begin{bmatrix} A & B \\ C & D \end{bmatrix} = \begin{bmatrix} \cos\beta\ell & jZ_o \sin\beta\ell \\ \frac{j}{Z_o} \sin\beta\ell & \cos\beta\ell \end{bmatrix} \tag{A.1}$$

and V_S, I_S are input voltage and current (I_S into port) and V_R, I_R are output voltage and current (I_R out of port). These two-port equations can be applied to Figure A.2 such that for the k^{th} turn of an N-turn rotary transformer:

$$\begin{bmatrix} V_1^{(k)} \\ I_1 \end{bmatrix} = \begin{bmatrix} A_a & B_a \\ C_a & A_a \end{bmatrix} \cdot \begin{bmatrix} V_2^{(k)} \\ I_o \end{bmatrix} \tag{A.2}$$

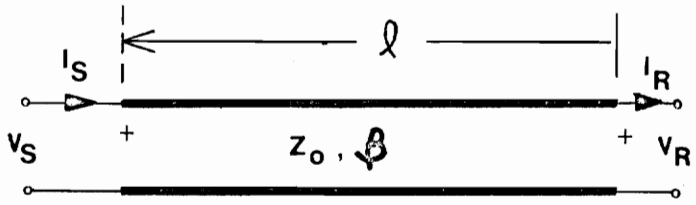

Figure A.1 Balanced current transmission line configuration

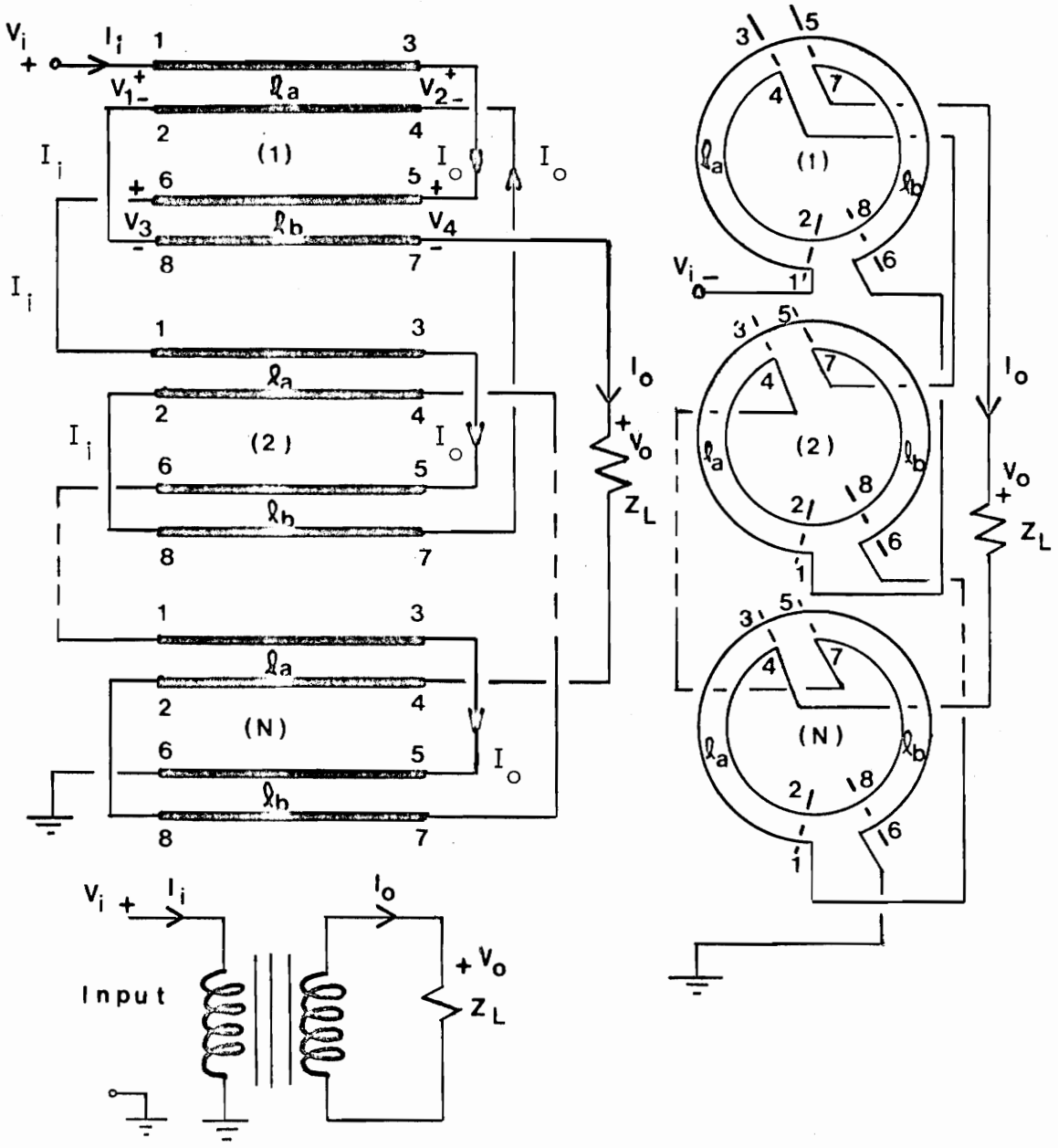

Figure A.2 Transmission line circuit for rotating transformer

and

$$\begin{bmatrix} V_3^{(k)} \\ \\ I_i \end{bmatrix} = \begin{bmatrix} A_b & -B_b \\ \\ -C_b & A_b \end{bmatrix} \cdot \begin{bmatrix} V_4^{(k)} \\ \\ I_o \end{bmatrix} \tag{A.3}$$

The "a" and "b" subscripts indicate that the equations apply to line segments having lengths ℓ_a and ℓ_b respectively.

The input and output terminal voltages of the rotary transformer configuration in Figure A.2 are expressed by

$$V_i = \sum_{k=1}^{N} [V_1^{(k)} - V_3^{(k)}] \tag{A.4}$$

$$V_o = \sum_{k=1}^{N} [V_2^{(k)} - V_4^{(k)}] \tag{A.5}$$

Equations (A.2) and (A.3) can be used to express (A.4) and (A.5) in terms of the network input and output currents such that

$$V_1^{(k)} = \frac{A_a}{C_a} I_i - \frac{I_o}{C_a} \tag{A.6}$$

$$V_2^{(k)} = \frac{I_i}{C_a} - \frac{A_a}{C_a} I_o \tag{A.7}$$

$$V_3^{(k)} = \frac{I_o}{C_b} - \frac{A_b}{C_b} I_i \tag{A.8}$$

$$V_4^{(k)} = \frac{A_b}{C_b} I_o - \frac{I_i}{C_b} \tag{A.9}$$

The input and output currents (I_i and I_o) are the same for each winding because of the balanced current assumption. So long as all windings are identical then regardless of rotation:

$$V_1^{(1)} = V_1^{(2)} = \ldots = V_1^{(N)} \tag{A.10}$$

$$V_2^{(1)} = \ldots = V_2^{(N)} \tag{A.11}$$

$$V_3^{(1)} = \ldots = V_3^{(N)} \tag{A.12}$$

$$V_4^{(1)} = \ldots = V_4^{(N)} \tag{A.13}$$

Now (A.4) and (A.5) can be expressed as:

$$V_i = N\,[V_1 - V_3] \tag{A.14}$$

and

$$V_o = N\,[V_2 - V_4] \tag{A.15}$$

The transmission equations of the N-turn rotary transformer configuration are derived from a substitution of (A.6) thru (A.9) into (A.14) and (A.15). The result is that

$$V_i = \frac{A_a C_b + A_b C_a}{C_a + C_b} \cdot V_o + \frac{N(B_a C_b + C_a B_b + 2A_a A_b - 2)}{C_a + C_b} I_o \tag{A.16}$$

$$I_i = \frac{C_a C_b}{N (C_a + C_b)} \cdot V_o + \frac{A_a C_b + A_b C_a}{C_a + C_b} I_o \tag{A.17}$$

It can be determined from (A.16) and (A.17) that the rotary transformer is bilateral and symmetrical regardless of rotation. Therefore, either the stator or rotor could serve as a signal input or output.

Equations (A.16) and (A.17) can be expressed in terms of transmission line parameters as

$$V_i = \frac{\sin \beta (\ell_a + \ell_b)}{\sin \beta\ell_a + \sin \ell_b} V_o + \frac{j N Z_o [2 - 2 \cos \beta (\ell_a + \ell_b)]}{\sin \beta\ell_a + \sin \beta\ell_b} I_o \qquad (A.18)$$

and

$$I_i = \frac{j \sin \beta\ell_a \sin \beta\ell_b}{N Z_o \sin \beta\ell_a + \sin \beta\ell_b} V_o + \frac{\sin \beta (\ell_a + \ell_b)}{\sin \beta\ell_a + \sin \beta\ell_b} I_o \qquad (A.19)$$

If the output is loaded with impedance Z_L so that

$$V_o = I_o Z_L, \qquad (A.20)$$

then the input impedance is expressed by

$$Z_i = Z_o \frac{N Z_L \sin \beta (\ell_a + \ell_b) + j N^2 Z_o [2 - 2 \cos \beta (\ell_a + \ell_b)]}{N A_o \sin \beta (\ell_a + \ell_b) + j Z_L \sin \beta\ell_a \sin \beta\ell_b} \qquad (A.21)$$

The insertion loss is calculated to be

$$\frac{P_{av}}{P_o} = E/F \qquad (A.22)$$

where

$$E = (Z_L + Z_o)^2 N^2 \sin^2 \beta (\ell_a + \ell_b) + \{Z_L \sin \beta\ell_a \sin \beta\ell_b + Z_o N^2 [2 - 2 \cos \beta (\ell_a + \ell_b)]\}^2 \qquad (A.23)$$

and

$$F = 4\, Z_L\, Z_o \{N^2 \sin^2\beta\, (\ell_a + \ell_b) - N^2\, [2 - 2\cos\beta\, (\ell_a + \ell_b)]\cdot \sin\beta\ell_a \sin\beta\ell_b\}. \qquad (A.24)$$

APPENDIX B

Unbalanced Transmission Line Theory Applied to the Rotary Transformer

The analysis of the rotating transmission line transformer for instances when unbalanced currents are present is aided by the theory of earlier work [12, 13, 14, 15, 17]. In particular, Sato [12] proposed a very useful matrix to describe the unbalanced transmission line illustrated in Figure B.1.a. This matrix is expressed by

$$\begin{bmatrix} V_{1\ell} \\ V_{2\ell} \\ I_{1\ell} \\ I_{2\ell} \end{bmatrix} = \begin{bmatrix} x_1 & x_2 & z_1 & z_2 \\ x_2 & x_1 & z_2 & z_1 \\ y_1 & y_2 & x_1 & x_2 \\ y_2 & y_1 & x_2 & x_1 \end{bmatrix} \begin{bmatrix} V_{10} \\ V_{20} \\ I_{10} \\ I_{20} \end{bmatrix} \tag{B.1}$$

where $x_1 = (\cosh \gamma_u \ell + \cosh \gamma_o \ell)/2$

$$x_2 = (\cosh \gamma_u \ell - \cosh \gamma_o \ell)/2$$

$$z_1 = Z_u \sinh \gamma_u \ell + \frac{Z_o}{4} \sinh \gamma_o \ell$$

$$z_2 = Z_u \sinh \gamma_u \ell - \frac{Z_o}{4} \sinh \gamma_o \ell \tag{B.2}$$

$$y_1 = \frac{1}{4Z_u} \sinh \gamma_u \ell + \frac{1}{Z_o} \sinh \gamma_o \ell$$

$$y_2 = \frac{1}{4Z_u} \cdot \sinh \gamma_u \ell - \frac{1}{Z_o} \sinh \gamma_o \ell$$

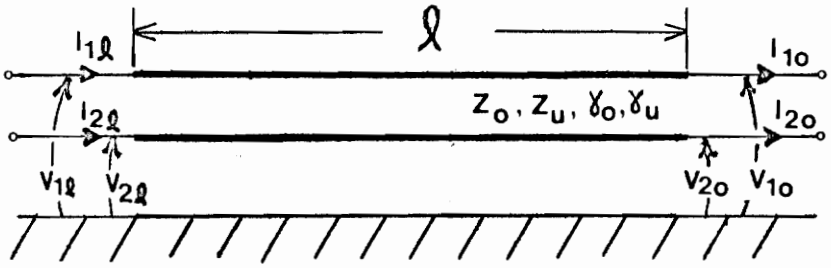

Figure B.1.a Unbalanced transmission line

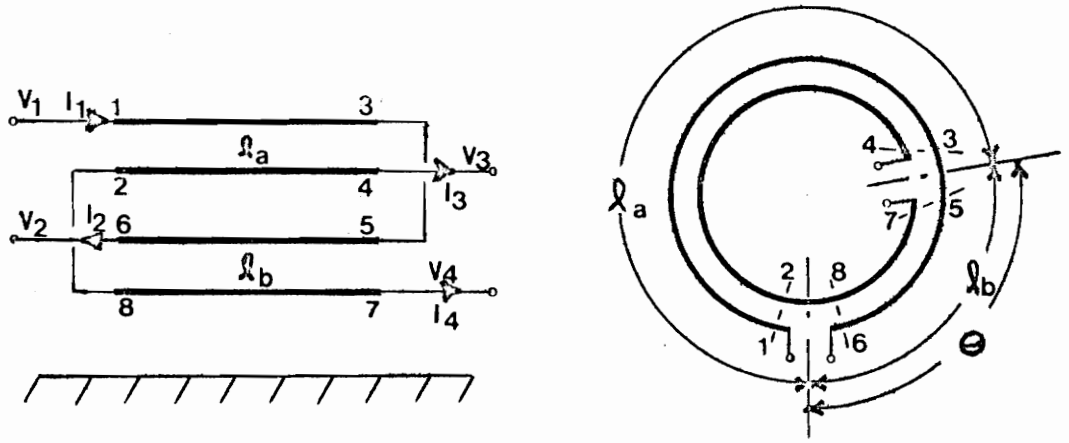

Figure B.1.b Unbalanced transmission line circuit formed during rotation (voltages are referenced to ground plane)

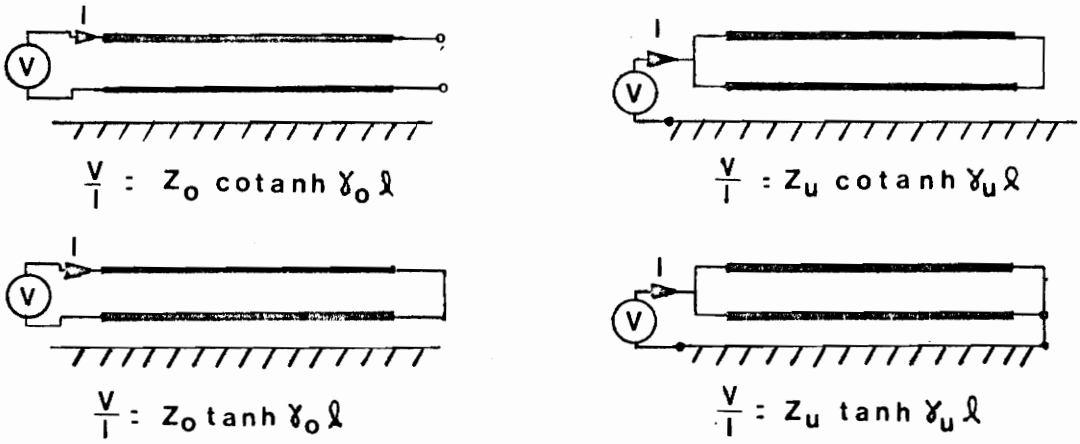

Figure B.1.c Connection for measuring transmission line parameters

and

$$\gamma_o = \alpha + j\beta$$

$$\gamma_u = \alpha_u + j\beta_u \ .$$

Two transmission line modes exist on the two wire line when unbalanced currents are present. This is indicated by the two propagation constants and by the two characteristic impedances Z_o and Z_u, the balanced and unbalanced current characteristic impedances respectively.

The inverse of (B.1) is sometimes useful and is expressed by

$$\begin{bmatrix} V_{10} \\ V_{20} \\ I_{10} \\ I_{20} \end{bmatrix} = \begin{bmatrix} x_1 & x_2 & -z_1 & -z_2 \\ x_2 & x_1 & -z_2 & -z_1 \\ -y_1 & -y_2 & x_1 & x_2 \\ -y_2 & -y_1 & x_2 & x_1 \end{bmatrix} \begin{bmatrix} V_{1\ell} \\ V_{2\ell} \\ I_{1\ell} \\ I_{2\ell} \end{bmatrix} \tag{B.3}$$

From experiment it has been determined that wide band transformers in general tend to be lossless in the balanced mode if the line length is short and good dielectrics are used. Under this condition

$$\gamma_o = j\beta \tag{B.4}$$

and

$$\begin{aligned} \sinh \gamma_o \ell &= j \sin \beta\ell \\ \cosh \gamma_o \ell &= \cos \beta\ell \ . \end{aligned} \tag{B.5}$$

Equations (B.1) and (B.4) can be applied to the rotary transformer turn configuration depicted in Figure B.1.b. The rotating structure forms two transmission lines during rotation each having length ℓ_a and ℓ_b. The rotation angle, θ, is related to ℓ_a and ℓ_b by

$$\theta = \frac{2\pi\ \ell_b}{\ell_a + \ell_b} \quad (\theta \text{ in radians}) \tag{B.6}$$

The sum in the denominator of (B.6) is constant during rotation and is the length of a single transformer turn. The parameters Z_o, Z_u, γ_o, and γ_u can all be measured for the rotary transformer when $\theta = 0$, using the connections of Figure B.1.c.

The values of Z_o, Z_u, γ_o, and γ_u are determined [18] from the short circuit and open circuit parameters obtained by the measurement techniques illustrated by Figure B.1.c:

$$\begin{aligned} Z_o &= \sqrt{Z_{oc}\ Z_{sc}} \\ Z_u &= \sqrt{Z_{oc}'\ Z_{sc}'} \end{aligned} \tag{B.7}$$

where

$$\begin{aligned} Z_{oc} &= Z_o \ \text{cotanh}\ \gamma_o\ell \\ Z_{sc} &= Z_o \ \tanh\ \gamma_o\ell \\ Z_{oc}' &= Z_u \ \text{cotanh}\ \gamma_u\ell \\ Z_{sc}' &= Z_u \ \tanh\ \gamma_u\ell \end{aligned} \tag{B.8}$$

Also,

$$\tanh\ \gamma_o\ell = \sqrt{\frac{Z_{sc}}{Z_{oc}}} = A + jB \tag{B.9}$$

and

$$\tanh \gamma_u \ell = \sqrt{\frac{Z_{sc}'}{Z_{oc}'}} = A' + jB', \tag{B.10}$$

and it can be shown that

$$\alpha\ell = \frac{1}{2} \tanh^{-1}\left(\frac{2A}{A^2 + B^2 + 1}\right) \tag{B.11}$$

$$\beta\ell = \frac{1}{2} \tan^{-1}\left(\frac{2B}{1 - A^2 - B^2}\right) + \frac{M\pi}{2} \tag{B.12}$$

$$\alpha_u\ell = \frac{1}{2} \tanh^{-1}\left(\frac{2A'}{(A')^2 + (B')^2 + 1}\right) \tag{B.13}$$

$$\beta_u\ell = \frac{1}{2} \tan^{-1}\left(\frac{2B'}{1 - (A')^2 - (B')^2}\right) + \frac{L\pi}{2} \tag{B.14}$$

where M and L are integers.

The equations of a single turn can be shown to be

$$\begin{bmatrix} V_1 \\ V_2 \\ I_1 \\ I_2 \end{bmatrix} = [G] \begin{bmatrix} V_3 \\ V_4 \\ I_3 \\ I_4 \end{bmatrix} \tag{B.15}$$

where [G] is given in Table I. Note that the "a" and "b" subscripts indicate that terms from (B.1) and (B.2) have line lengths ℓ_a and ℓ_b. The matrix expressed by (B.15) is applicable to the analysis of several connections made with the rotary transformer. Two of interest are the 1:1 balun type hookups depicted by Figure B.2. Each, in general, could have N turns. A prototype was built with five turns. The boundary conditions for connection I and N = 5, (see Figure B.2.) are that:

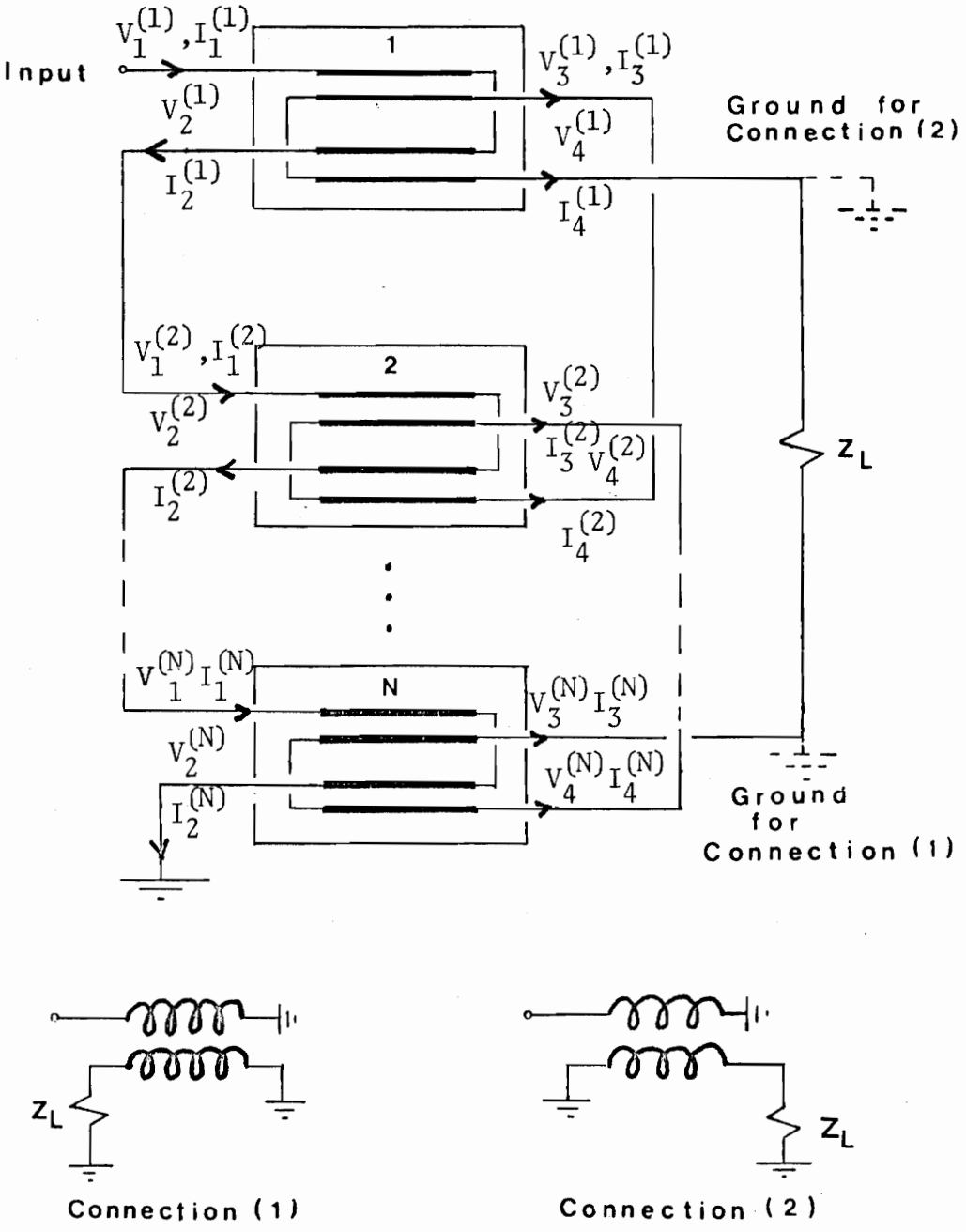

Figure B.2 Terminal conditions for rotary transformer connections

$$
\begin{aligned}
&V_2^{(1)} = V_1^{(2)} \quad V_3^{(1)} = V_4^{(2)} \quad I_3^{(1)} = -I_4^{(2)} \quad I_2^{(1)} = I_1^{(2)} \\
&V_2^{(2)} = V_1^{(3)} \quad V_3^{(2)} = V_4^{(3)} \quad I_3^{(2)} = -I_4^{(3)} \quad I_2^{(2)} = I_1^{(3)} \\
&V_2^{(3)} = V_1^{(4)} \quad V_3^{(3)} = V_4^{(4)} \quad I_3^{(3)} = -I_4^{(4)} \quad I_2^{(3)} = I_1^{(4)} \\
&V_2^{(4)} = V_1^{(5)} \quad V_3^{(4)} = V_4^{(5)} \quad I_3^{(4)} = -I_4^{(5)} \quad I_2^{(4)} = I_1^{(5)} \\
&V_2^{(5)} = 0
\end{aligned}
\tag{B.16}
$$

also

$$
\begin{aligned}
&V_3^{(5)} = 0 \\
&V_i = V_1^{(1)} \\
&I_i = I_1^{(1)} \\
&V_o = V_4^{(1)} \\
&I_o = I_4^{(1)}
\end{aligned}
\tag{B.17}
$$

The position of the output ground can be relocated to form connection 2. For this case it is necessary to change the terminal boundary conditions such that

$$
\begin{aligned}
&I_o = -I_3^{(5)} \\
&V_o = -V_3^{(5)} \\
&V_4^{(1)} = 0.
\end{aligned}
\tag{B.18}
$$

Letting $V_1^{(1)}$ be the independent variable, twenty equations result for a 5-turn device. In general using (B.7), four equations and four unknown quantities result per turn. The equations also will change with

rotation. Consequently, due to this and the system size, solution must be obtained on a digital computer. Results are discussed in Chapter IV.

Table I. Elements of [G] (equation (B.15))

1) $$g_{11} = x_{2a} - \frac{x_{1a}}{D}\left[y_{1a}(z_{2a} + z_{2b}) + z_{1a}(y_{2a} + y_{2b}) + \frac{(x_{2a} + x_{2b})}{D} \cdot \left[x_{1a}^2 + y_{1a} z_{1a}\right]\right.$$

2) $$g_{12} = \frac{x_{1b} z_{1a}}{D}(y_{2a} - y_{2b}) - \frac{y_{1b} x_{1a}}{D}(z_{2a} + z_{2b}) - \frac{(x_{2a} - x_{2b})}{D} \cdot \left[x_{1a} x_{1b} - y_{1b} z_{1a}\right]$$

3) $$g_{13} = z_{2a} - \frac{x_{1a}^2}{D}(z_{2a} + z_{2b}) - \frac{z_{1a}^2}{D}(y_{2a} + y_{2b}) + 2\left(\frac{x_{2a} - x_{2b}}{D}\right) x_{1a} z_{1a}$$

4) $$g_{14} = \frac{z_{1a} z_{1b}}{D}(y_{2a} + y_{2b}) - \frac{x_{1a} x_{1b}}{D}(z_{2a} + z_{2b}) + \left(\frac{x_{2a} - x_{2b}}{D}\right)\left[z_{1a} x_{1b} - x_{1a} z_{1b}\right]$$

5) $$g_{21} = \frac{x_{1a} z_{1b}}{D}(y_{2a} + y_{2b}) - \frac{x_{1b} y_{1a}}{D}(z_{2a} + z_{2b}) + \frac{x_{2a} - x_{2b}}{D}\left[x_{1a} x_{1b} - y_{1a} z_{1b}\right]$$

6) $$g_{22} = x_{2b} - \frac{x_{1b}}{D}\left[z_{1b}(y_{2a} + y_{2b}) + y_{1b}(z_{2a} + z_{2b})\right] - \left(\frac{x_{2a} - x_{2b}}{D}\right)\left[x_{1b}^2 + y_{1b} z_{1b}\right]$$

7) $$g_{23} = \frac{z_{1a} z_{1b}}{D}(y_{2a} + y_{2b}) - \frac{x_{1a} x_{1b}}{D}(z_{2a} + z_{2b}) + \frac{x_{2a} - x_{2b}}{D}\left[z_{1a} x_{1b} - x_{1a} z_{1b}\right]$$

8) $$g_{24} = z_{2b} - \frac{z_{1b}^2}{D}(y_{2a} + y_{2b}) - \frac{x_{1b}^2}{D}(z_{2a} + z_{2b}) - 2\left(\frac{x_{1b} z_{1b}}{D}\right)(x_{2a} - x_{2b})$$

Table I (continued)

9) $$g_{31} = y_{2a} - \frac{y_{1a}^2}{D} \cdot (z_{2a} + z_{2b}) - \frac{x_{1a}^2}{2} \cdot (y_{2a} + y_{2b}) + 2\,\frac{x_{1a}\,y_{1a}}{D}\,(x_{2a} - x_{2b})$$

10) $$g_{32} = \frac{x_{1a}\,x_{1b}}{D}\,(y_{2a} + y_{2b}) - \frac{y_{1a}\,y_{1b}}{D}\,(z_{2a} + z_{2b}) + \left(\frac{x_{2a} - x_{2b}}{D}\right)\left[x_{1a}\,y_{1b} - y_{1a}\,x_{1b}\right]$$

11) $$g_{33} = x_{2a} - \frac{x_{1a}}{D}\left[z_{1a}\,(y_{2a} + y_{2b}) + y_{1a}\,(z_{2a} + z_{2b})\right] + \left(\frac{x_{2a} - x_{2b}}{D}\right)\left[x_{1a}^2 + z_{1a}\,y_{1a}\right]$$

12) $$g_{34} = \frac{z_{1b}\,x_{1a}}{D}\,(y_{2a} + y_{2b}) - \frac{x_{1b}\,y_{1a}}{D}\,(z_{2a} + z_{2b}) + \left(\frac{x_{2a} - x_{2b}}{D}\right)(x_{1a}\,x_{1b} - z_{1b}\,y_{1b})$$

13) $$g_{41} = \frac{y_{1a}\,y_{1b}}{D}\,(z_{2a} + z_{2b}) - \frac{x_{1a}\,x_{1b}}{D}\,(x_{2a} - x_{2b}) + \left(\frac{x_{2a} - x_{2b}}{D}\right)\left[y_{1a}\,x_{1b} - x_{1a}\,y_{1b}\right]$$

14) $$g_{42} = -y_{2b} + \frac{y_{1b}^2}{D}\,(z_{2a} + z_{2b}) + \frac{x_{1b}^2}{D}\,(y_{2a} + y_{2b}) + 2\,\frac{x_{1b}\,y_{1b}}{D}\,(x_{2a} - x_{2b})$$

15) $$g_{43} = \frac{y_{1b}\,x_{1a}}{D}\,(z_{2a} + z_{2b}) - \frac{x_{1b}\,z_{1a}}{D}\,(y_{2a} + y_{2b}) + \left(\frac{x_{2a} - x_{2b}}{D}\right)\left[x_{1a}\,x_{1b} - y_{1b}\,z_{1a}\right]$$

Table I (continued)

16) $$g_{44} = -x_{2b} + \frac{x_{1b}}{D}\left[y_{1b}\,(z_{2a} + z_{2b}) + z_{1b}\,(y_{2a} + y_{2b})\right] + \left(\frac{x_{2a} - x_{2b}}{D}\right)\left[x_{1b}^{2} - y_{1b}\,z_{1b}\right]$$

also: $$D = (y_{2a} + y_{2b})\,(z_{2a} + z_{2b}) - (x_{2a} - x_{2b})^{2}$$

BIBLIOGRAPHY

1. C. L. Ruthroff, "Some Broadband Transformers," Proc. IRE, 47: 1337-1342, August, 1959.

2. O. Pitzalis and Thomas P. Couse, "Broadband Transformer Design for RF Transistor Power Amplifiers," U.S. Army Technical Report, ECOM-2989.

3. O. Pitzalis, R. E. Horn, and R. J. Baranello, "Broadband 60-W HF Linear Amplifiers," IEEE Journal of Solid-State Circuits, Vol. SC-6, No. 3, June, 1971.

4. O. Pitzalis, and T. P. Couse, "Practical Design Information for Broadband Transmission Line Transformers," Proc. IEEE, pp. 738-739, April 1968.

5. Magnetic Circuits and Transformers. M.I.T. Staff, John Wiley and Sons, Inc., 1943.

6. Ferroxcube Magnetic Design Manual, Ferroxcube Corporation: Saugerties, New York, 1971.

7. Solid State Power Circuits. RCA Technical Series SP-52, pp. 482-488, Harrison, New Jersey, 1971.

8. Ferroxcube Linear Ferrite Materials and Components. Feroxcube Corporation: Saugerties, New York, 1971.

9. R. C. Hejhall, "Solid State Linear Power Amplifier Design," Motorola AN-546, Motorola Semiconductor Products, Inc.

10. O. Mueller, "Low Distortion Wideband Transistor Power Amplifier," 1972 International Symposium on Circuit Theory, North Hollywood, California.

11. E. F. Sartori, "Hybrid Transformers," IEEE Transactions on Parts, Materials and Packaging, Vol. PMP-4, No. 3, September, 1968.

12. I. Otawara and R. Sato, "Characteristics of the DC Cut-off Transmission-type Transformer," Electrical Engineering in Japan, Vol. 87, No. 7, July, 1967.

13. Y. Shimada, "Input Impedance Analysis of 1:1 Balun," IEEE Transactions on Microwave Theory and Techniques, Vol. MIT-18, No. 5, May 1970.

14. Y. Shimada, "Fundamental Considerations of Broadband Line Type Transformers," Review of The Electrical Communication Laboratory, Vol. 18, No. 1-2, Jan.-Feb., 1970.

15. A. Talkin and J. Cuneo, "Wideband Balun Transformer," Rev. Sci. Inst. Vol. 28, p. 808, October, 1957.

16. E. C. Snelling, Soft Ferrites. Mullards Research Laboratories. Chemical Rubber Co. Press, 1969.

17. Yokogawa and Sato, "Transformer Using Bifilar Helices and its Application," IEEE, Japan, Vol. 82, p. 758, 1962.

18. P. C. Magnusson. Transmission Lines and Wave Propagation. Allyn and Bacon, Inc.: Boston, 1971.

VITA

Charles W. Allen was born April 25, 1947, in Staunton, Virginia. He received his primary level education at Beverly Manor Elementary School and his high school education at Buffalo Gap High School, both schools being located near Staunton, Virginia. During his senior year in high school he won recognition at local, regional, and national-international science fairs. He received the Bachelor of Science degree in Electrical Engineering from Virginia Polytechnic Institute in 1969. In March, 1971, he received the MSEE degree at the University of Tennessee. In March of 1971 he began work toward the Doctor of Philosophy degree in Electrical Engineering at Virginia Polytechnic Institute.

In the summer of 1974 he received a NASA Summer Research Fellowship for work at NASA, Houston.

Mr. Allen is a member of Eta Kappa Nu and a registered professional engineer in Virginia.

Charles W. Allen

WIDEBAND ROTARY TRANSFORMER FOR VHF USE

by

Charles W. Allen

(ABSTRACT)

This report describes a device which transmits wideband VHF signals across a rotating structure. It has potential application to antenna systems which rotate and also to telemetry between stationary and rotating structures.

No electrical contact is necessary between stationary and rotating terminals. The bandwidth typically is 1000:1 and the device can be designed to operate from a few megahertz to well up into the VHF band.

A successful prototype has been developed which verifies the device theory.